TECHNICAL MEMORANDUMS

NATIONAL ADVISORY COMMITTEE FOR AERONAUTICS

No. 557

MEASUREMENT OF PROFILE DRAG ON AN AIRPLANE IN FLIGHT BY THE MOMENTUM METHOD

By Martin Schrenk

PART I

From Luftfahrtforschung, May 18, 1928

Washington
March, 1930

NATIONAL ADVISORY COMMITTEE FOR AERONAUTICS.

TECHNICAL MEMORANDUM NO. 557.

MEASUREMENT OF PROFILE DRAG ON AN AIRPLANE IN FLIGHT BY THE MOMENTUM METHOD.*

By Martin Schrenk.

PART I.

I. Introduction

In order to measure the forces exerted on bodies by flowing fluids, the reaction pressures are usually transmitted to balances by suitable devices. Owing to the nature of this direct method of measurement, it is restricted to models of certain sizes, as determined by the dimensions of the testing apparatus. Of course, water-tank tests with full-size airplanes and other large bodies are not technically impossible but, on account of the great difficulties encountered, the tests are usually confined to small models.

The conversion of these results to full-size airplanes entails certain difficulties. The coefficients of geometrically similar bodies, as determined by tests according to the quadratic law of flow resistance (law of inertia), cannot be expected to hold good for all sizes and velocities, since the viscosity effects do not follow this law. The drag coefficients can be accu-

*"Ueber Profilwiderstandmessung im Fluge nach dem Impulsverfahren" from Luftfahrtforschung, May 18, 1928; subsequently published in the 1929 Yearbook of the Deutsche Versuchsanstalt für Luftfahrt, pp. 9-40.

rately converted only in cases of similarity of the flow diagrams. Theoretically this takes place when the ratio of the inertia effect to the viscosity effect remains constant in the flow (Reynolds law of similarity) or, in other words, when the flow velocity multiplied by the comparative length and divided by the "kinematic viscosity" (that is, by the Reynolds Number) gives a constant quantity. This purpose is fulfilled in practice by the product of the flow velocity and the comparative length alone (Reynolds Number), since the kinematic viscosity is usually constant enough.

For ordinary air-flow measurements, where the linear dimensions of the model are roughly from 1/10 to 1/25 and the attainable velocities approximately 1/2 to fully those of an actual airplane, Reynolds Number always differs so greatly from that of the full-size airplane that the convertibility of the results is impaired. The resulting uncertainty is, however, of no great importance, owing to the moderate degree of accuracy of ordinary airplane performance calculations. Test results must nevertheless be accurate, in order to keep pace with the gradual improvement of airplane structures which (entirely apart from its scientific importance) greatly affects the economical value and the efficiency of very large airplanes.

A further consideration applies to wings. According to air-flow measurements, their drag consists of induced drag, inseparably connected with the production of lift, and of profile drag,

which depends on the shape of the model. The former is roughly calculated by Prandtl's wing theory, while the latter is obtained by subtracting the induced drag from the total measured drag. For great lift values it forms only a fraction of the induced drag. Since it is a difference between two values of the same order of magnitude, the results are greatly affected by small errors in both values. It is therefore particularly desirable to find means for directly determining this portion of the wing drag.

This requirement is fulfilled by a method, published three years ago, by A.Betz, Göttingen (Reference 1). This method dispenses with the determination of any dynamic effects on the body itself. It is based on the assumption that the pressure and momentum losses of the flow caused by the body must enable an accurate calculation of the drag. These losses occur in a region behind the body usually designated as the vortex trail. Therefore, variations of pressure and momentum are measured instead of forces, whence the expression "momentum method."

This method is not affected by the size of the measured body. On the contrary, the accuracy of the drag measurement increases with the size of the vortical region. This method is particularly suited to full-size airplane measurements. The drag of airplane parts, especially of wing sections, can thus be directly determined, whereas soaring-flight measurements give the total airplane drag as a function of the lift derived from

the flight speed and from the angle of the flight path or vertical velocity. The method was first tested in actual flight by H. Weidinger (Reference 2) in the summer and autumn of 1925. However, owing to lack of time after completing the installation, he could make only one preliminary test with a Junkers corrugated sheet-metal wing.

In November, 1925, the writer was entrusted with the continuation of the tests. Before the necessary changes and reinforcements had been fully tried out in preliminary tests, the airplane was badly damaged in a cross-country flight and was not completely repaired until the middle of May, 1926. The first report of the tests was made in the middle of June in the form of a short paper read at the meeting of the W. G. L. In September, 1926, some of the most important results were communicated to a small number of people in the form of a Preliminary Report of the D. V. L. Toward the end of 1926 the tests had to be discontinued on account of other work undertaken by the writer.

The present report contains the results thus far obtained and is intended to form the basis of further tests. Absolute accuracy is not claimed for the values given in this report. They present, however, a series of noteworthy viewpoints for investigation.*

*In this connection I wish to thank my assistants, the pilots Nippert and Walter Hübner, for their skillful cooperation in making the rather difficult test flights. I am also greatly indebted to Mr. Stippler and other students of the Berlin Technical High School for their efficient assistance in the tedious numerical interpretation of the photographs.

II. The Method

a) Notation

p	kg/m^2,	static pressure (pressure energy per unit of space) at any point of flow.
q	kg/m^2,	dynamic pressure (kinetic energy per unit of space) at any point of flow ($q = \rho/2\ v^2$).
g	kg/m^2,	total pressure at any point of flow ($g = p + q$).
g_o	kg/m^2,	total pressure of (potential) flow outside of vortical region.
p_∞	kg/m^2,	static pressure of unaffected (infinitely distant) flow (it being assumed for practical reasons that $p_\infty = 0$).
q_∞	kg/m^2,	dynamic pressure of unaffected (infinitely distant) flow ($q_\infty = g_o$, since $p_\infty = 0$).
q_i	kg/m^2,	"ideal" dynamic pressure of imaginary potential flow inside of vortical region ($q_i = (g_o - g) + q$). Also see corresponding explanation in section b).
v	m/s,	flow velocity.
W	kg,	flow resistance.
l	m,	width of wing portion considered.
t	m,	thickness of wing portion considered.
F	m^2,	plan area of wing portion considered ($l\ t$).
G	kg,	weight of the airplane.
ρ	$\frac{kg/s^2}{m^4}$,	density of fluid.
γ	$\frac{kg}{m^3}$,	weight of fluid.
β^o,		angle of longitudinal inclination of airplane.
A,B,C,D,E,		auxiliary values, as explained in text.

b) Derivation of Formulas

The theoretical bases and the derivation of the formulas were given by Betz in his fundamental publication (Reference 1). Nevertheless, it seems advisable to give another presentation of these relations in a form more readily understood by engineers.

1. Every flow has a certain amount of energy. Bernoulli's law, according to which the sum of the static and kinetic energies* per unit volume is constant and equal to the total energy per unit volume

$$p + q = g \qquad (1)$$

holds good as long as the flow is free from losses or vortices (potential flow).**

When an actual fluid flows past a body, the always present viscosity, however small, retards the fluid layer next to the surface of the body, and the retarded particles form a vortex trail behind the body. The flow energy of this trail is obviously less than that of the free flow. The dynamic pressure q drops and no corresponding increase in the static pressure takes place. Hence their sum, the total pressure $\cdot$ g, is smaller in this case than in the undisturbed potential flow (Fig. 1).

*This refers to free vortices. Restrained vortices, that is, those which have streamlines coinciding with the vortex lines (circulation about a wing), are not opposed to the conditions of potential flow.

**Neglecting the potential energy, i.e., the elevation of each individual fluid element.

The energy thus withdrawn from the flow must reappear in the drag exerted on the body. Hence, if the energy lost by the flow could be measured, it would afford a means of determining the drag of the body. Unfortunately, this does not lead to the desired end. A nonreversible transformation of energy takes place in turbulent flow. Under the influence of internal friction the energy of the vortices is gradually converted into heat which cannot be measured.

2. These difficulties are overcome by the application of the momentum law of fluid flow. This law does not deal with energy, but only with force and momentum. Hence it also applies without restriction to flows with energy losses.* Its adaptation to the present conditions reads as follows (Fig. 2): "Considering the conditions in two planes (control planes) perpendicular to the direction of the flow, forward and aft of a drag-producing body, the force exerted by the flow on the body is equal to the difference between the static pressures in the two planes plus the difference between the momentums of the fluid masses flowing through the two planes per unit of time."

In other words, every obstacle withdraws from the flow a certain momentum per second and also changes its static pressure. The sum of the two changes is equivalent to the force exerted on the body. (Note in this connection that the momentum is a

*The practical difficulties of making technically reliable pressure measurements in the turbulent zone are disregarded at first.

vector.) For subsequent derivatives let the distance between the control planes and the body be so chosen as to insure a sufficient parallelism of the streamlines between the control planes. It is also assumed that the drag-producing body has a sufficient lateral extension, so that the flow may be regarded as smooth. It is assumed, moreover, that the body produces no lift at first.

The momentum (Fig. 2) which passes through the surface element $l\,dy$ per second, is

$$\rho\, v^2\, l\, dy,$$

provided v is the velocity of flow at the point considered. This "transmittal of momentum" has the dimension of a force. The total momentum variation per second

$$\rho\, l \int_{-\infty}^{+\infty} (v_0^2 - v^2)\, dy,$$

is obtained by integration of the momentum transmittal over the fore (index 0) and aft (without index) planes and by forming the difference between the two planes.

Hence the total pressure difference in the two planes is

$$l \int_{-\infty}^{+\infty} (p_0 - p)\, dy.$$

The body drag, according to the momentum equation, then, is

$$W = l \int_{-\infty}^{+\infty} (p_0 - p)\, dy + \rho\, l \int_{-\infty}^{+\infty} (v_0^2 - v^2)\, dy \qquad (2)$$

3. This expression is technically valueless, since measurements cannot be carried on indefinitely. It must be endeavored

to transform both integrals so as to confine them to a small finite zone. The obvious way is to adopt the vortex trail as such a zone, since the most important phenomena take place in it.

This can be easily effected for the first integral by splitting off half of the second integral and adding it to the first. According to equation (1),

$$\left(p_o + \frac{\rho}{2} v_o^2\right) - \left(p + \frac{\rho}{2} v^2\right) = g_o - g.$$

However, in the potential flow outside the vortex trail (Fig. 1), $(g_o - g)$, the difference between the total pressures, becomes zero. Then equation (2) reads

$$W = l \int (g_o - g)\, dy + \frac{\rho}{2} l \int_{-\infty}^{+\infty} (v_o^2 - v^2)\, dy \qquad (3)$$

The first integral now contains the total pressure losses. As stated above, these cannot, however, be considered offhand as the total energy losses. It will be shown later that this integral plays numerically the most important part, while that of the second member is gradually reduced with increasing distance between the after control plane and the drag body to be tested.

The second integral must be further transformed in order to become measurable. Betz achieves this result by an ingenious expedient. He introduces sources at the rear end of the body which produce additional velocities in the vortical region.* The magnitude of these additional velocities is so proportioned

*Regarding "sources" see Hütte I, 25th edition, chapter on Hydrodynamics (Betz).

at each point that the actual potential flow, outside the turbulent zone, is supplemented by an imaginary potential flow in this zone. In other words, the total pressure of the flow in the turbulent region is again raised at each point to the level of the total pressure outside the turbulent region* by adding $(g_0 - g)$ to its dynamic pressure q, thus raising it to q_i (Fig. 3). The magnitude of the imaginary velocity produced by the source flow is v_i. v_i and v coincide outside the turbulent region.

According to the above statements the output of this flow is

$$E = l \int (v_i - v)\, dy.$$

It follows from an equation, analogous to the lift equation of Kutta and Schukowsky, that in a translational flow with a velocity v_∞, the source flow produces a negative drag of the magnitude

$$W_Q = - \rho\, v_\infty\, E = - \rho\, l \int v_\infty\, (v_i - v)\, dy \qquad (4)$$

This drag W_Q can also be determined by applying to the imaginary potential flow with a source, the same considerations which led to equations (2) and (3). In this case the drag of the source flow is

$$W_Q = \frac{\rho}{2}\, l \int_{-\infty}^{+\infty} (v_0^2 - v_i^2)\, dy \qquad (5)$$

since the total pressure, inside the potential flow, remains constant and the first integral is consequently eliminated.

*Since constancy of the total pressure is a characteristic feature of potential flow.

Hence, according to equations (4) and (5)

$$-\rho\, l \int v_\infty\,(v_i - v)\,dy = \frac{\rho}{d}\, l \int_{+\infty}^{-\infty} (v_o^2 - v_i^2)\,dy \qquad (6)$$

This equation is then subtracted from equation (3) in order to eliminate the troublesome difference $(v_o^2 - v^2)$.

$$W + \rho\, l \int v_\infty\,(v_i - v)\,dy = l \int (g_o - g)\,dy + \frac{\rho}{2}\, l \int (v_i^2 - v^2)\,dy \qquad (7a)$$

whence, by a simple transformation, we finally obtain the formula indicated by Betz:

$$W = l \int (g_o - g)\,dy - \frac{\rho}{2}\, l \int (v_i - v)\,(2\,v_\infty - v_i - v)\,dy \qquad (7)$$

In this case the second integral likewise disappears outside the turbulent region, since v_i and v differ from each other only in the turbulent region.

By a second deduction, made in exactly the same way, in which a downward velocity w is added to the velocity v in the after control plane, Betz shows that the result is not affected by a simultaneous production of lift.

4. Equation (7) is still very unsatisfactory, since it requires the determination of the air density and the calculation of three flow velocities. The roots of the corresponding dynamic pressures are therefore substituted for these velocities and, after division by the wing area and the dynamic pressure of the infinitely remote flow, the following expression is obtained.

$$c_w = \frac{W}{F\, q_\infty} = \frac{1}{t\, q_\infty}\left\{ \int (g_o - g)\, dy - \right.$$

$$\left. - \int (\sqrt{q_i} - \sqrt{q})\, (2\sqrt{q_\infty} - \sqrt{q_i} - \sqrt{q})\, dy \right\} \qquad (8)$$

The rating of the flights was based on this formula.*

c) Determination of the Different Quantities

1. Before going into details, we shall explain briefly how pressure measurements are made in flowing mediums. Figure 4 shows two standard static tubes (Reference 4). Both have a central bore which ends in the forward point of symmetry. In the case of an axial air flow the total pressure is measured at this point, as the sum of the static and dynamic pressures. The static pressure alone is measured on the side of the tube, at a point where the pressure is equal to that at the mouth of a tube with the flow at the same velocity. The difference between the two pressures is the dynamic or impact pressure.

For practical reasons, the static pressure of the free unaffected flow (p_∞) is here put at zero, as is often done in practical aerodynamics. In this unaffected flow the dynamic pressure q_∞ is then equal to the total pressure g_o. However, as soon as the flow velocity v_o at the point of measurement

*The writer endeavored to simplify this member in order to lessen the work of rating. The results were reported at the W.G.L. meeting in the summer of 1926. This method was subsequently abandoned, however. It was found that, owing to the distance of the static tubes from the trailing edge of the wing, the correction member still materially affected the result. Owing to the inaccuracy of the correction member, the simplification caused a slight increase in the values, which had to be avoided for the sake of absolute accuracy.

deviates from v_∞, the impact pressure q_o also changes, while $g_o = q_\infty$ at every point in the potential flow.

2. q_∞, the dynamic pressure of the infinitely remote flow cannot be measured directly, since the flow in the neighborhood of the airplane is affected by it, and hence the static pressure everywhere differs from that of the free atmosphere.* This circumstance necessitates a correction of the dynamic-pressure readings of Pitot tubes mounted on airplanes, which is usually determined by flight-speed measurements from the ground. Another method was adopted in the present case, since the greatest gliding speed attained during the tests greatly exceeded the horizontal speed of the airplane.

The static tube was installed where a constant minimum static pressure could be expected at all flight speeds, and where, moreover, the static pressure could be calculated with a fair degree of accuracy. This was achieved by installing the tube (tube I, Fig. 5) at a distance of about two wing chords above the leading edge of the wing (in agreement with Prandtl's simple wing theory). Under these conditions the flow is rotated in the same direction during variations of the angle of attack, whereby the effect of the latter on the readings is reduced.

*The static pressure of the unaffected flow might be determined with sufficient accuracy by means of a static sounding device towed far beneath the airplane. The carrying of the sounding device, however, is attended by certain disadvantages and would jeopardize the safety of the airplane, if it were not pulled up before landing. Moreover, its indications are not reliable at high speeds, since it then has a tendency to oscillate.

The static pressure was calculated at this point according to Prandtl's wing theory on the assumption of the horseshoe vortex. The calculation was checked by a flight with the static sounding device, and the agreement between the two results was satisfactory. The magnitude of the pressure difference between the free flow and the point of measurement was, in both cases, about 4 mm on the alcohol pressure gauge.* Thus q_∞ is very accurately determined, which is important on account of its great effect on the calculated result.

3. $(g_o - g)$, the difference between the total pressures, is the most important value next to q_∞. g_o was recorded by tube I, and g by tube II (Fig. 5). As already mentioned, the variation in the angle of attack near tube I kept within such narrow limits that its effect on the test results could be disregarded. In most cases tube II was of the Brabbée type. It recorded total pressures without being affected by quite large inclinations (Fig. 6). Owing to certain considerations outlined in 4, a Prandtl tube was also used for some of the measurements, as will be explained below. For the following reason, this tube is likewise unaffected by variations of the angle of attack.

Tubes II and III were placed in the mean direction of the flow prevailing at their point of installation. This direction varies a few degrees from the flight direction due to deviations

*This static pressure difference is independent of the lift coefficient, since the weight of the airplane and its dimensions are constant (variations in the lift distribution being disregarded).

in the flow under the action of the lift produced by the wing. Strictly speaking, therefore, a component of the profile drag is measured in this case. Practically, however, its magnitude agrees with the actual value, owing to its small angular deflection.

The mean direction of flow was determined by woolen threads fastened beside the Pitot tubes. While the variation in the angle of attack of the wing, within the range of the test speeds, amounted to about 9°, as determined by transferring the lift coefficients to the polar diagram (Reference 2), the variation in the angle of flow, as indicated by the woolen threads, was estimated at about 5°, thus being much smaller. Hence the Prandtl tube could not be greatly affected by variations in the angle of attack.

4. Therefore, the variations of the mean direction of flow in the vortex trail are of no practical importance. We shall now briefly consider the deviations from the mean direction, due to burble vortices. These vortices introduce transverse velocities into the flow. The direction of the resultant flow, at a given fixed point of the airplane, will therefore oscillate irregularly about the mean direction.

Since the momentum is a vector, the devices used for its measurement should record only the component coinciding with the direction of flight, which is not a pressure component but the component of the local velocity raised to the fourth power.

Hence a tube had to be used, the readings of which vary as the square of the angle of inclination.

This does not apply to the Brabbée tube, since up to about 20°, it is nearly insensitive to angular deflections (Fig. 6).* On the other hand, according to Figure 6, the normal Prandtl tube with a bore/diameter ratio of 0.3 fully satisfies this requirement up to about 20°. Hence a Prandtl tube was used instead of a Brabbée tube for certain measurements (flights 25, 26, 30, 31).

These measurements were expected to produce a slightly greater drag than those made with a Brabbée tube. Hence, according to the above consideration and owing to the lack of angular sensitivity of the Brabbée tube, its momentum measurements in the vortex trail were too large, and the difference in comparison with the potential flow was therefore too small. The result, however, was negative. The measurements made with the Prandtl tube did not yield uniformly greater values than those obtained with other tubes. The smallest drag coefficients ever determined were, in fact, measured with the Prandtl tube. We might thus be led to believe that the angular deflections in the vortex trail never attain values worth mentioning. This conclusion, however, should be adopted with caution, since the actual conditions have not yet been sufficiently explained.

*The Brabbée tube was originally adopted because of its lack of sensitivity to errors of inclination.

5. q, the dynamic pressure in the after control plane, is measured with a Prandtl tube (tube III, Fig. 5). The dynamic-pressure readings of such a tube are independent of the angle of attack of the flow within quite a wide range (Reference 4). Logically, the considerations of No. 3 also apply to this case. This influence is negligible, however, owing to the small numerical value of the second integral.

6. As stated in Section II, b, 3, q_i is derived from q by addition of the total pressure drop

$$q_i = q + (g_o - g).$$

7. The exact position of the two Pitot tubes, located behind the wing, is shown in Figure 7. Their distance from the trailing edge is about 30% of the wing chord. This accounts for the comparatively large part (1/5 to 1/8) of the second integral in the total result. It might be objected that the wing chord opposite the two tubes is not the same. Owing to the fact, however, that the drag coefficient was calculated for the portion of the wing located in front of the Brabbée tube, this small error affects the correction member only and can be practically disregarded. The distance of the measuring instruments from their supports is sufficient to prevent the latter from disturbing the flow.

d) The Testing Installation

On the whole, the original arrangement (Reference 2) was satisfactory. Its main part consists of a vertical graduated bar located behind the wing. A slide carrying the Pitot tubes for the measurement of the pressures in the turbulent zone can be moved along this bar from the observer's cockpit. The pressures are recorded by U-shaped alcohol pressure gauges of which motion pictures are taken. Before and during the present tests, a number of changes and improvements were made. They are briefly recorded below, since they embody, in part, the results of measuring tests.

1. The new position of the Pitot tube for the measurement of the undisturbed flow (tube I) has already been mentioned in c, 2. The Pitot tube (Fig. 8) is mounted on a braced mast above and slightly to the right of the fuselage. When entering a hangar, the mast can be let down, after loosening a turnbuckle. The original arrangement of the forward Pitot tubes on the left wing, which showed a tendency to vibrate in harmony with the wing, was abandoned.

2. In order to avoid the influence of the rail and of the tube holder, the support of the rear Pitot tubes (Fig. 9) was extended and reinforced. A new slide with a wide copper guide was provided and fitted without play, in order to fix the position of the Pitot tubes more accurately. The notches in the

slide-guide and the pawl, catching every 25 centimeters, served the same purpose. (During the first flights the slide had a tendency to shift.)

The rubber tubes were made as short as possible. Besides, at the points exposed to the free air flow, they were protected by steel-wire spiral springs to avoid pinching, which otherwise frequently occurred.

3. The control board in the observer's cockpit (Fig. 10) was raised, in order to reduce the absolute inclination of the U-tubes, which had to be perpendicular to the sighting line of the motion-picture camera. The board was blackened in order to avoid undesirable reflections. A narrow white strip was placed behind each alcohol column to form a better background than the black board. The scales behind the U-tubes were eliminated and a scale made of an aluminum strip 200 mm long was secured to the middle of the board. The readings of the rear Pitot tubes were originally marked with chalk on the board. This primitive method was replaced by a small roller box provided with a slot in which all the readings of the Pitot tube were shown by turning a button.

4. The motion-picture camera (kindly supplied by the Askania Works) had a lens of great focal length (Zeiss-Tessar f 3.5; F = 5 cm) to enable using the full size of the film. The pictures were taken on a diapositive film (Fig. 11) which has a finer grain than ordinary films. Still, the slight haze

caused by vibration could never be completely avoided, so that the particular advantages of the diapositive film were never fully realized. Some of these changes may seem unimportant, but the degree of success of the tests actually depends on such trifles, after the general arrangements have been definitely settled.

III. The Tests

a) Method of Testing

The airplane adopted for the tests was a two-seated low-wing Junkers with a B.M.W. IV engine, type A 20, like the one used by Weidinger (Reference 2). While Weidinger made his measurements with a more or less throttled engine, the present tests were made only in gliding flight. This method avoids disturbances due to the propeller slipstream and insures steadiness of the liquid columns in the pressure gauges, owing to absence of engine vibrations.

The following method suggested by Madelung was adopted for the execution of the tests. The pilot made a gliding flight with the pressure gauges in a given altitude position, beginning at maximum speed and slowing down gradually to minimum speed. These flights depended greatly on the skill of the pilot, but did not, on the other hand, require the position of the Pitot tubes to be changed during the test. Moreover, it is not easy to maintain absolutely uniform speed, as would otherwise be necessary.

In this way 10 to 15 such soaring flights had to be made, according to the width of the turbulent region and the distance of the different positions of the Pitot tubes. After some practice the flights were quite successful. The plotting of a polar required a flight of 35 to 50 minutes, from take-off to landing.

The U-tubes were photographed during the gliding flights. The author endeavored at first to catch the right moment when the liquid columns were at rest. In the course of uniform gliding flights, however, the best results were obtained by turning the motion-picture film slowly and uniformly. The oscillations of the liquid columns, especially for pressure indication in the turbulent region, were so jerky that the moments of rest were usually over before the operator began to turn the handle.

The effect of accelerations will be further discussed in Section III, e. The measurements must of course be made in absolutely undisturbed air. To this end, it was often necessary to climb through low clouds, above which particularly steady air currents often prevailed. The flight altitude was between 1000 and 3000 m (3280 and 9840 ft.).

The upper limit of the test speed was set by controllability considerations, its lower limit being determined by the incipient separation of the flow, which rendered steady flight impossible. Besides, the speed could not be reduced to the same figure with all kinds of covering, since rough surfaces

caused very pronounced premature separation phenomena.

b) Interpretation of the Photographs

The pictures were projected on a screen and the position of the alcohol columns measured directly with a metric scale. The above-mentioned fixed calibration range made an accurate setting of the scale easy. The evaluation was greatly facilitated by using a scale of 1 : 1. The values were recorded in tables (See Table I) prepared for the purpose. In order to simplify this table, formula (8),

$$c_w = \frac{1}{t\, q_\infty} \left\{ \int (g_o - g)\, dy - \right.$$

$$\left. - \int \left(\sqrt{q_i} - \sqrt{q}\right) \left(2\sqrt{q_\infty} - \sqrt{q_i} - \sqrt{q}\right) dy \right\}$$

upon which the table is based, was altered and condensed as follows: The integrals were made nondimensional by dividing by q_∞. This division eliminates the effect of the variable longitudinal inclination of the airplane on the indications of the alcohol columns.* This also eliminates the density of the liquid used. The measurement and calculation are greatly simplified and certain sources of errors are avoided by the elimination of these two factors.

Formula (8) now becomes

$$100\, c_w = \frac{1}{t} \int (A - B)\, dy$$

*The figures in columns 1 to 3 are not pressures in millimeters of alcohol column, but their components which vary with the longitudinal inclination or with the flight speed. The effect of the longitudinal inclination on the calculation of the lift coefficients is dealt with in Section III,d.

where

$$A = \frac{100}{C}(g_o' - g') \quad \text{and} \quad B = \frac{100}{C} D E.$$

C is a dynamic pressure which differs from q_∞ by the density γ of the gauge liquid and by the influence of the angle of longitudinal inclination β. As compared with the measured dynamic pressure q_o', C already incorporates a correction of 4 mm alcohol column,* due to the position of Pitot tube I (Section II,c,2).

$$C = q_o' - 4 \left(= \frac{q_\infty}{\gamma \cos \beta}\right).$$

Moreover,

$$D = \sqrt{q_i'} - \sqrt{q'} \quad \text{and} \quad E = 2\sqrt{C} - (\sqrt{q_i'} + \sqrt{q'}).$$

Table I was computed from these values. This part of the evaluation work was purely mechanical and could therefore be done by the younger members of the force.

c) Representation of the Results

In accordance with the somewhat unusual method adopted for making the test flights, the representation of the results also differs from the usual method. Its choice furthermore is influenced by the fact that the individual values vary greatly, so that the finding of a mean value appears necessary for obtaining reasonable final results.

---

*Due to the smallness of the angle of inclination, its effect on this pressure difference is disregarded.

The relative pressure differences A - B (denoted by $\frac{\Delta p}{q}$ in the diagrams) were plotted against the parameter 100/C. This parameter is proportional to the lift coefficient, except for the effect of the longitudinal inclination of the airplane. Series of points are thus obtained which correspond, in each case, to a certain position of the Pitot tube with respect to the wing (Figs. 12 to 24).

Next, these series of points have to be grouped into series of curves. Obviously, this cannot be done by calculation, owing to the great number of points and to their irregular distribution. The only possible way consisted in drawing mean curves, according to the appearance, through the different series of points. The accuracy attainable by this method is discussed farther on. In most cases, the series of curves thus obtained could be easily supplemented by an enveloping curve.

These series of curves represented a good mean of the measured values. They were then cut by vertical lines corresponding to a series of lift coefficients. The ordinates, obtained by the intersection of these lines with the individual curves, were plotted, in the second instance, over the position y of the Pitot tubes, and the pressure loops drawn accordingly (Figs. 25 to 36). The drag coefficients were obtained by measuring the areas of these loops with a planimeter.

d) Calculation of the Lift Coefficients

The lift coefficients of the tested wing portion could not be measured accurately, since this would have required pressure measurements about holes bored through the wing. The simplified assumption was therefore adopted that the coefficient of this wing portion equals the mean lift coefficient of the whole wing, an assumption which seems justified by the small importance of c_a in the present measurements. For this case the formula is

$$c_a = \frac{G}{F\, q_\infty} \tag{9}$$

The most important factor is the flying weight G, this being the most easily variable value. To avoid weighing before each flight, the fuel tanks were replenished each time, and the airplane was always left in the same condition in other respects. The mean flying weight, for an average duration of 3/4 of an hour, was about 1400 kg. The wing area of the A 20 is 30.5 m² (328 sq.ft.). According to the preceding paragraph, the dynamic pressure q_∞ is

$$q_\infty = C\, \gamma \cos\beta \tag{10}$$

During one of the first flights the angle of longitudinal inclination β was determined as a function of C by the longitudinal inclinometer. With the aid of this function the relation between q_∞ and C was established once for all. The specific gravity of the alcohol was $\gamma = 0.81$.

e) Accuracy of Measurement

Accuracy of measurement will now be considered, while the reliability of the momentum method, as such, will be discussed further on.

1. The readings of the alcohol column were accurate to within ±0.5 mm. For the dynamic pressure this represents, at a mean pressure of 100 mm, an error of ±0.5%, while for the difference in the total pressures, at a mean pressure of 25 mm, it represents an error of ±2%. The resulting discrepancies are not systematic.

2. After calibration, the coefficient of the Pitot tubes could be represented accurately enough by 1. The total pressure measurement, which is not much affected by the shape of the tubes, is the main contribution to the result (Reference 4). The resulting error is constant but does not exceed 1%.

3. According to Section II, c, 2, the determination of the velocity of the infinitely remote flow (v_∞) is made with a fair degree of accuracy. In this case the error does not exceed 1%.

4. The longitudinal inclination of the airplane and the density of the liquid used for the measurement are not important, since they are eliminated by division of the pressures and consequently do not have to be taken into consideration in the calculation of the drag coefficients (Section III, b).

5. Lateral inclinations of the airplane were indicated by a special short closed U-tube and immediately subtracted from

the measured values while the readings were being taken.

6. The influence of the acceleration might be important, since the flights were made over a curved course. Although sudden accelerations were avoided, absolutely steady flight was almost impossible, owing to the continual variation of speed.

It is obvious, however, that continuous accelerations cannot affect the result. When, during an acceleration, the pilot flies at a constant angle of attack and hence with a constant lift coefficient, the wing loading and the dynamic pressure increase in the same ratio as the acceleration, according to the equation of equilibrium normal to the flight path. The specific gravity of the alcohol increases in the same proportion, so that the relation between the dynamic pressure and the readings remains constant. The same results are obtained in the case of constant dynamic pressure. The only thing to be feared are jerky accelerations due to unlike dynamic conditions of the different alcohol and air columns after being set in motion.

Analysis of the results showed that the points of accelerometer deflection did not differ systematically from the points where no acceleration was indicated. It may also be noted that, according to reliable observation, the variations of the readings in the vortical region, which are sometimes considerable, are due to turbulence of the air and not to accelerations of the airplane.

7. The determination of the points in the first diagram by free-hand curves may seem arbitrary. Anybody who does it carefully, however, finds that the series of points usually affords a rather clearly defined curve, provided the points are not too scattering. Often when the whole diagram seems confusing, the difficulty can be easily overcome by plotting separately the series of points corresponding to one position of the Pitot tube.

The following short statement shows the numerical importance of even slight differences in the drawing of these curves. Each loop of the second diagram is equivalent to a rectangle with a base equal to that of the loop and an altitude approximately half the maximum height of the loop or numerically about $0.13 \frac{\Delta p}{q}$ (Fig. 37). The average length of the base of this rectangle is 15 cm. Since the different positions of the Pitot tubes are 2.5 cm apart, there are about 6 points for each loop. The effect of a small variation δ of one of the points, due to an error in the drawing of the first diagram, is then

$$E = \frac{1}{6} \frac{\delta}{0.13} = 1.3.$$

Figures 12 to 24 (See Appendix, Part II) show that in changing the direction of the curves of the first diagram at any point by $\delta = 0.02 \frac{\Delta p}{q}$ there results a rather pronounced deflection from the seemingly correct line. This, however, causes an error of only 2.5%. In addition to this fact, such a variation in the direction of a curve causes an opposite variation in the

neighborhood, at least along the central portion of the curve. This partly offsets the error. (The determination at the wing tips is often much less correct, especially since the scattering of the points increases greatly at large c_a values. Thus, maximum accuracy of the curves is achieved within the range of mean lift coefficients.)

The same consideration naturally applies to the drawing of loops of the second diagram. The shape of these loops is not always clearly defined by 6 points, but still accurately enough for the enclosed area to be scarcely affected by possible variations in the direction of the curves.

In endeavoring, on the strength of this consideration, to estimate numerically the possible error made in plotting the curves, it should be kept in mind that the scattering of the points changes greatly for each flight according to the roughness of the wing surface. The accuracy depends of course on this mean scattering. Therefore, ±3% can be assumed as the lower limit of the error (e.g., for flights 7, 15, 18) and from ±6% to 8% as the upper limit (e.g., flights 8 and 20). As already mentioned, this excludes values relating to very large and very small lift coefficients.

Attention is called to the absolute continuity of polars 14, 15, 18, 21, obtained for the same covering, and to the good agreement between polars 22 A and B, 29 A and B, 32 A and B, obtained during the same flight with mean lift coefficients.

The deflections of these curves at the ends are partly systematic and seem to be due to flow phenomena.

8. On summarizing paragraphs 1 to 7, it appears that, according to the range of the measured values, the method of calculations may be expected to have an accuracy of from ±5 to 10% within the range of the mean lift coefficients.

9. The method is a static process, the accuracy of which, according to the law of probability, increases with the number of points and the reduction of the scattering. In the present case an average of 350 points was required to plot a series of curves. This figure can be reduced under favorable conditions, but has to be increased when the points are broadly scattered. This leaves about 25 to 50 points to each curve. This number of points enables a rather close approximation, especially since it can be assumed that the unsystematic errors largely offset one another.

IV. The Results

a) Testing Program

The purpose of the present tests was the investigation of the effect produced, by varying the nature of the covering, on the air forces acting on a thick wing section. The different surface conditions were obtained by different wing coverings. This slightly altered the original shape of the wing section, owing to lack of perfect conformity of the covering. The duralu-

min covering conformed best, while the plywood covering I (Fig. 38) gave the poorest results.

It was proposed to test:

1. Original state of wing (Junkers corrugated sheet metal).
2. Plywood of different degrees of smoothness, obtained by varnishing.
3. Fabrics with different dopes (stretched over plywood).
4. Smooth sheet metal, bare and varnished.

The tests of item 2, due to the long time covered by the tests, were made twice. Tests 3 were made with the second covering.

The following items were added during the tests:

5. Roughening with poppy seed.
6. Wavy and battered sheet metal.
7. Effect of rows of rivets.

According to the Göttingen method, item 5 comprises a numerical definition of roughness which is used for comparative tests.

Item 6 is the result of an unsuccessful attempt to cover the wing with soft aluminum sheet of 0.5 mm thickness. The sheet was very uneven as is shown in Fig. 39. In spite of this fact, a test was made which forms a useful supplement to the other test results.

The necessity of investigating item 7 was only realized during the tests and therefore failed to receive systematic attention. The sheet-metal covering used in this connection is

shown in Figures 43 and 44. It had to be made from 0.9 mm duralumin strips, 0.5 m wide and 2 m long, since no larger pieces could be procured. Transverse seams had to be avoided as much as possible on the upper wing surface. This produced the arrangement shown in Figure 7 in which a line of rivets parallel to the direction of flight lay half-way between the Pitot tubes, while one of the corresponding transverse seams lay at the leading edge directly below the point of full dynamic pressure and the other 0.5 m from the trailing edge where the boundary layer is quite pronounced. Besides, the rivets of this last seam were countersunk for a distance of about 30 cm in front of each Pitot tube. The results proved clearly that the measured values are affected by the rivets. The results obtained, after removing the rivet heads and smoothing the seams, closely approached the conditions of absolutely smooth sheets which it had been sought to obtain.

b) The Coverings

It is not easy to fit such coverings on tapered wings. The plywood used for this purpose was 1.5 mm thick. The plywood sheet, 4.5 m long and 1.5 m wide, was first glued to a smooth band which was drawn wet over the wing and, while still wet, was joined together at the trailing edge with a wedge-shaped strip. The lower surface was finally pressed against the wing at the two edges by means of strips. The first covering did not con-

form satisfactorily to the leading edge and the lower surface sagged considerably (Fig. 40). The second covering, which was drawn tighter and was provided on the lower surface with internal formers, conformed very well (Figs. 41 and 42).

The failure of the first sheet-metal covering has already been mentioned. The covering of thicker sheet duralumin also caused certain difficulties, because the sheet was subjected to a stamping process at the riveting points and hence evinced a tendency to become distorted. Therefore, the rivets were hammered very lightly. Besides, the sheet gets bent easily and cannot be fully smoothed out again. Nevertheless, this covering conformed fairly well, at least to the particularly important upper surface. This was facilitated by the great camber of the Junkers wing section (Figs. 43 and 44).

c) The Test Results

The 22 successful flights are summarized in Table II. This makes it unnecessary to tabulate the 8344 test points shown on the film. There have been substituted instead a number of first and second diagrams selected from the characteristic cases and arranged according to their mutual correspondence.

Figures 12 to 24 show the points plotted from the motion pictures and converted according to Section III,b.* The pressure loops, obtained by cutting the series of curves thus developed, are shown in Figures 25-36. Lastly, the profile drag

*The ordinate $\Delta p/q$ corresponds to the quantity (A - B).

coefficients, obtained by planimeter measurement of these pressure loops, are plotted in the form of polars in Figures 45 to 51, where the abscissas are forty times the ordinates. The numerical values of the lift and drag coefficients are given in Table III. The range of measurement lies usually between c_a = 0.3 and c_a = 1.

The results are discussed below in greater detail.

d) Remarks on the Results

1. In general, the scattering of the points in Figures 12 to 24 toward the right end of the diagrams corresponding to large lift coefficients is an outstanding feature. It indicates an increasing separation of vortices and causes, as already explained in Section III, a certain decrease in the accuracy of the measurements at large lift coefficients. Also there is usually a slight loss of accuracy at the lower limit of the measured lift coefficients, since the curves which connect the points of the first diagram are then no longer "supported" by points on both sides.

The way in which the test points are determined naturally increases the continuity of the polars. Nevertheless, there frequently occur unusual phenomena such as the peculiar bifurcation of the polars of flight 29 and 32 (Fig. 50).

2. Measurements with a Junkers corrugated metal sheet and with a wavy smooth sheet showed a distinct difference in the

character of the polar.* At large lift coefficients the drag coefficients of the wavy smooth sheet are considerably smaller than those of the Junkers sheet, while there is a good agreement within the range of mean lift coefficients. Also, according to the first diagram (Figs. 12 and 13) the corrugated sheet produces a much greater turbulence than the wavy smooth sheet in the region of large lift coefficients. This difference in their behavior may be explained as follows.

At small lift coefficients, the flow on the upper and lower sides of the wing is practically parallel to the corrugations of the sheet, which at first caused only a slight increase of the area (Section V,f). However, at large c_a values, when the flow velocity above the wing greatly exceeds that below the wing, the air flows against the airplane axis on the upper side of the wing and away from it on the lower side.** Hence, on both sides, the direction of flow differs from that of the corrugations. The flow is forced to jump the corrugations with consequent formation of vortices and a corresponding increase in drag.

3. The smooth plywood covering I (Fig. 46) has the same remarkably straight polars as the plywood covering II (Fig. 47) at mean lift coefficients. Besides, the great regularity of

*The two measurements with the Junkers wing do not fully agree. The discrepancies are probably due to the fact that the whole testing installation was dismounted between the first and the second test, so that the transverse position of the Pitot tubes with respect to the corrugations may have been slightly altered.
**The cause of the turbulent area behind the wing. The deflection of the flow, however, is too small to affect the result.

curves 6, 7, 14, and 15 shows that the flow conditions about these two coverings must have been favorable. The decrease in drag with increasing smoothness is very regular.

On the whole, the characteristics of the plywood covering II are somewhat inferior to those of the plywood covering I. Besides, the region of constant drag coefficients is higher. This may be due to the greater unevenness, the greater relative thickness and to the smaller camber of covering I (Section IV,b).

In flight 15, the particularly quiet flow, due to the great smoothness of the polished plywood, gave values up to $c_a = 1.1$ (Fig. 15), although at this limit the points are greatly confused. There is a remarkably large gap between curves $y = 15$ and $y = 17.5$. It seems as though the flow would suddenly reverse in this region. Similar phenomena were observed during several flights. The small drag coefficients of flight 15 are surprising. The best profile lift-drag ratio is 125 for $c_a = 1$.

4. The polars of the doped fabric covering (flights 18 and 21) which were stretched over the plywood and therefore had no sag between the ribs, agree very well with the results obtained with the smooth plywood covering. Flights 16 and 20, in which the fabric, a raw inflation linen, was rather coarse, gave quite different results. Figures 16 and 17 (flight 20) particularly tax the ingenuity of the investigator. In order to obtain mean figures of some practical value despite the confusion of the points of measurement, their number was considerably increased

in the present case and they were plotted on two sheets. The results are not, however, entirely satisfactory, but the diagram clearly shows the marked turbulence throughout the whole range of measurement of the flow behind the wing.

5. Flight 22 begins the series of so-called double flights (flights 28, 29 and 32). They consisted of soaring flights carried out in the usual way at decreasing speed, each flight being followed by one at increasing speed, the position of the static tubes remaining unchanged. The purpose of these flights was, on the one hand, the creation of absolutely identical test conditions for checking the continuity of the estimates while, on the other hand, they were intended to determine whether the increase or decrease of the angle of attack during the measurement had any systematic effect on the result. The fact that these two aspects of the problem are not contradictory can probably be assumed if the results are continuous and can be reobtained. The polars flown in the usual way are denoted by A and those flown in the opposite direction by B.

The first diagrams (Figs. 23 and 24) of the first flight (No. 22) with this sheet-metal covering was already marked by conspicuous discontinuities in the curves y = constant. Considering the great smoothness of the sheet, the drag coefficients were surprisingly large. The polars had a peculiar S shape. After a few flights (Nos. 23, 25, 26), all the rivet heads were filed off and the remaining unevennesses smoothed out. The re-

sults of the following flights show a material reduction in the drag.

These polars are also marked by certain peculiarities. The forking of the two polars of the double flight 29, at $c_a = 0.6$, was confirmed by flight 32 (Fig. 50). Moreover, the systematic differences between these two pairs of polars are attributable to the fact that a full month had elapsed between the two flights. During this time the surface of the wing may have been slightly changed by dust and other causes. All these measurements prove that the profile drag is highly sensitive to small surface changes.

It may be surprising that rivet rows 50 cm apart should exert such a considerable influence. According to the report by Betz at the 1926 session of the W.G.L., it was observed in the wind tunnel that disturbances due, for instance, to suspension wires, spread wedgelike toward the rear and may greatly impair the result. Therefore, it may be assumed in the present case that disturbances due to rivet rows spread fanlike over the surface of the wing and change the whole character of the flow.

6. During flights 25, 26, 30, and 31, the total pressure behind the wing was measured with a Prandtl tube instead of a Brabbée tube. As already mentioned (Section II,c,4), the theoretical considerations regarding the probable increase in the drag coefficients with this tube were not confirmed in practice.

Flights 26 and 31 were measured on the left cross section (in front of tube III in Fig. 7), and again confirm the sensitivity of the profile drag to small variations of shape.

Besides, the first plottings of flights 30 (Fig. 23) and 31 are remarkable for the particularly good continuity of the points of measurement. This may indicate that the Prandtl tube is particularly well suited for such measurements. It may, however, simply be due to the fact that the total pressure and the dynamic pressure were measured with one tube, whereas this was previously done at two different places (tubes II and III). The smallest values of the drag coefficients found for smooth seamless sheet-duralumin coverings are a little smaller than those of the polished plywood covering II (Section V,f).

7. Perhaps the most unexplainable phenomena are those of flights 23 and 33, particularly as regards the polar (Fig. 51), which has a peculiar S shape. We are as yet unable to say whether this behavior was originally due to the bronze paint or whether there were other causes which have been overlooked.

e) Remarks on the Reliability of the Momentum Method

The accuracy of this method was considered in Section III,b, where it was shown that it could occasion no important errors. On the other hand, it may still be doubted as to whether the momentum method, in itself, is absolutely reliable, i.e., whether it covers correctly all drag-producing losses of flow. This can

be determined only by tests.

The question as to whether the momentum was correctly measured inside the vortex trail by the above means seems to be answered in the affirmative by the tests with the Prandtl tube (Section II,c,4). However, caution is advisable on account of the mixed character of the flow in the vortical region, the internal structure of which has yet been but little investigated. This applies particularly to measurements at large lift coefficients, when the flow is greatly disturbed by its incipient separation. At decreasing lift the results of wind-tunnel measurements with symmetrical wing sections were found to agree well with the results of the usual methods of force measurement, at least at a considerable distance from the wing.*

Attention is also called to the fact that the profile drag is not necessarily constant throughout the whole span. Variations in the direction and the velocity of flow at the wing tips at large lift values (the cause of the vortex trail) may result in considerable differences between the drag values of otherwise geometrically similar profiles. Moreover, the effect of aileron slots and the rounding of the wing tips and fittings will probably cause the best results yet obtained to be somewhat exceeded by the coefficients of very smooth wings. In short, it may be said that perfect mathematical accuracy cannot yet be claimed

*According to recent Göttingen wing-section tests the method is quite reliable at distances exceeding 3t. At smaller distances, such as were adopted for the present measurements (approximately 0.3 t), discrepancies were found. However, the error does not generally exceed ±8%.

for the results obtained by the momentum method, but they are of great value as standards of comparison.

References

1. Betz, A. : "Ein Verfahren zur direkten Ermittelung des Profilwiderstands," Zeitschrift fur Flugtechnik und Motorluftschiffahrt, 1925, p.42. (See N.A.C.A. Technical Memorandum No. 337: A Method for the Direct Determination of Wing-Section Drag.)

2. Weidinger, H. : "Profilwiderstandsmessungen im Fluge," 1926 Yearbook of the Wissenschaftliche Gesellschaft für Luftfahrt.

3. Prandtl, L. : Ergebnisse der Aerodynamischen Versuchsanstalt zu Göttingen, Reports I and II, 1923.

4. Kumbruch, H. : "Messung strömender Luft mittels Staugeräten," Forschungsheft No. 240 des Vereins deutscher Ingenieure.

Translation by
National Advisory Committee
for Aeronautics.

Flight No. 30. TABLE I.

No. of reading	$g_o'-g$	q_o'	q'	q_i'	$\sqrt{q_i'}$	$\sqrt{q'}$	D	$\sqrt{q_i'}+\sqrt{q'}$
	①	②	③	④	⑤	⑥	⑦	⑧
	Reading			①+③	$\sqrt{④}$	$\sqrt{③}$	⑤-⑥	⑤+⑥
1	41	208	135	176	13.3	11.6	1.7	24.9
2	39	225	150	189	13.9	12.3	1.5	26.1
3	43	213	139	182	13.5	11.8	1.7	25.3
4	42	214	139	181	13.5	11.8	1.7	25.3
5	37	200	130	167	12.9	11.4	1.5	24.3
6	39	192	122	161	12.7	11.1	1.6	23.8
7	39	195	125	164	12.8	11.2	1.6	24.0
8	39	183	116	155	12.5	10.8	1.7	23.3
9	37	178	113	150	12.3	10.6	1.7	22.9
10	38	183	115	153	12.4	10.7	1.7	23.1
11	36	170	106	142	11.9	10.3	1.6	22.2
12	35	158	97	132	11.5	9.9	1.6	21.4
13	33	164	104	137	11.7	10.2	1.5	21.9
14	32	144	88	120	11.0	9.4	1.6	20.4
15	32	138	82	114	10.7	9.1	1.6	19.8
16	32	134	80	112	10.6	8.9	1.7	19.5
17	30	129	77	107	10.3	8.8	1.5	19.1

Flight No. 30 TABLE I (Cont.) Measuring point y = 27.5

No. of reading	C	$2\sqrt{C}$	E	$\frac{100}{C}$	A	B	A - B
	⑨	⑩	⑪	⑫	⑬	⑭	⑮
	② - 4	$2\sqrt{⑨}$	⑩ - ⑧	$\frac{100}{⑨}$	⑫ · ①	⑫ · ⑦ · ⑪	⑬ - ⑭
1	204	28.6	3.7	0.49	20.1	3.1	17.0
2	221	29.8	3.7	0.45	17.7	2.5	15.2
3	209	29.0	3.7	0.48	20.6	3.0	17.6
4	210	29.0	3.7	0.48	20.0	3.0	17.0
5	196	28.0	3.7	0.51	18.9	3.8	16.1
6	188	27.4	3.6	0.53	20.7	3.1	17.6
7	191	27.6	3.6	0.52	20.4	3.0	17.4
8	179	26.8	3.5	0.56	21.8	3.3	18.5
9	174	26.4	3.5	0.58	21.3	3.5	17.8
10	179	26.8	3.7	0.56	21.2	3.5	17.7
11	166	25.8	3.6	0.60	21.6	3.5	18.1
12	154	24.8	3.4	0.65	22.7	3.5	19.2
13	160	25.3	3.4	0.63	21.6	3.2	17.4
14	140	23.7	3.3	0.71	22.9	3.8	19.1
15	134	23.2	3.4	0.75	23.9	4.1	19.8
16	130	22.8	3.3	0.77	24.6	4.3	20.3
17	125	22.4	3.3	0.80	24.0	4.0	20.0

TABLE II. Summary of Rated Flights

Serial No.	Flight No.	Pilot	Wing covering	Remarks
1	5+9	Nippert	Junkers corrugated sheet	First successful flights
2	13	"	Junkers corrugated sheet	Supplementary flight
3	6	Nippert	Plywood I oiled	Brabbee and Prandtl tubes
4	7	"	" I varnished	
5	8	"	" I roughened with poppy seed	
6	14	Nippert	Plywood II oiled	
7	15	Hübner	" II varnished and polished	
8	16	Hübner	Plywood II with coarse fabric, taut	
9	20	"	Plywood II with coarse fabric, loose	
10	21	"	Plywood II with fabric twice doped, slightly polished	
11	18	"	Plywood II with fabric six times doped and polished	
12	11+12	Nippert	0.5 mm aluminum, uneven	
13	22 A	Hübner	0.9 mm duralumin with rivets	Gliding flights begun at high speed
14	22 B	Hübner	0.9 mm duralumin with rivets	Gliding flights begun at lowest speed
			With aluminum-bronze paint	
15	23	Hübner	0.9 mm duralumin with rivets	Brabbee and Prandtl tubes
16	25	Nippert	0.9 mm Duralumin with rivets	Prandtl tube alone, right
17	26	"	0.9 mm duralumin with rivets	Prandtl tube alone, left
18	29 A	Nippert	0.9 mm duralumin with rivet heads removed	Brabbee and Prandtl tubes
19	29 B			Gliding flights begun at lowest speed

TABLE II (Cont.)

Serial No.	Flight No.	Pilot	Wing covering	Remarks
20	30	Nippert	0.9 mm duralumin with rivet heads removed	Prandtl tube alone, right
21	31	"	0.9 mm duralumin with rivet heads removed	Prandtl tube alone, left
22	32 A	Hübner	0.9 mm duralumin with rivet heads removed	Brabbée and Prandtl tubes
23	32 B	"	0.9 mm duralumin with rivet heads removed With aluminum-bronze paint	Gliding flights begun at lowest speed
24	33	Nippert	0.9 mm duralumin with rivet heads removed	Brabbée and Prandtl tubes
25	34	"	0.9 mm duralumin with rivet heads removed	Only for pressure test outside vortical region

TABLE III. Profile Drag Coefficients (100 c_w)*

Flight	5+9	6	7	8	11+12	13	14	15
c_a = 0.3	1.13	1.10	0.81	1.88	1.12	1.18	0.99	0.84
0.4	1.16	1.15	0.84	1.94	1.14	1.13	0.93	0.76
0.5	1.15	1.14	0.85	1.94	1.17	1.09	0.94	0.71
0.6	1.14	1.15	0.85	1.90	1.20	1.08	0.93	0.70
0.7	1.30	1.14	0.88	2.36	1.27	1.14	0.90	0.71
0.8	(1.84)	1.28	1.04	-	1.36	1.37	0.93	0.71
0.9	(2.06)	1.46	1.12	-	1.55	1.67	1.06	0.74
1.0	-	-	1.15	-	1.86	(2.48)	(1.38)	0.80
1.1	-	-	-	-	-	-	-	(0.92)

TABLE III (Cont.)

Flight	16	18	20	21	22 A	22 B	23	25
c_a = 0.3	1.26	0.81	2.23	1.15	0.92	0.84	1.02	0.82
0.4	1.24	0.77	2.22	1.10	0.93	0.90	1.02	0.84
0.5	1.26	0.78	2.40	1.14	0.96	0.96	1.07	0.86
0.6	1.34	0.78	2.49	1.14	0.98	0.99	0.97	0.94
0.7	1.56	0.77	2.24	1.18	0.99	0.97	0.99	0.97
0.8	1.86	0.74	2.53	1.38	0.96	0.99	1.00	1.00
0.9	(1.68)	0.74	-	1.48	0.99	1.03	1.11	1.17
1.0	-	0.82	-	1.75	1.13	1.22	1.40	1.66

*Numbers in parentheses are not entirely reliable.

TABLE III. Profile Drag Coefficients (100 c_w). (Cont.)

Flight	26	29 A	29 B	30	31	32 A	32 B	33
c_a = 0.3	0.79	0.77	0.60	0.60	0.62	-	-	0.68
0.4	0.78	0.80	0.59	0.57	0.65	0.66	0.71	0.79
0.5	0.85	0.77	0.62	0.57	0.62	0.81	0.62	0.83
0.6	0.98	0.68	0.69	0.63	0.62	0.70	0.75	0.80
0.7	1.08	0.67	0.70	0.63	0.61	0.76	0.80	0.76
0.8	1.10	0.65	0.70	0.67	0.70	0.75	0.77	0.69
0.9	1.27	0.65	0.71	0.74	0.68	0.72	0.77	0.69
1.0	1.93	0.72	0.78	0.89	0.68	0.80	0.80	0.75

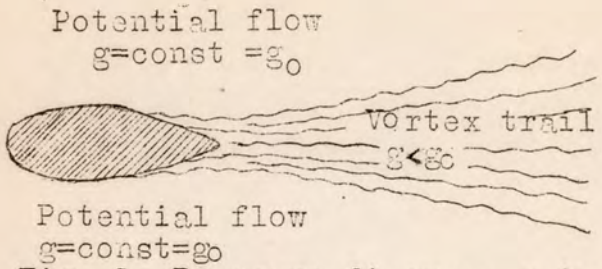

Fig. 1 Pressure diagram. g is constant outside the vortical region.

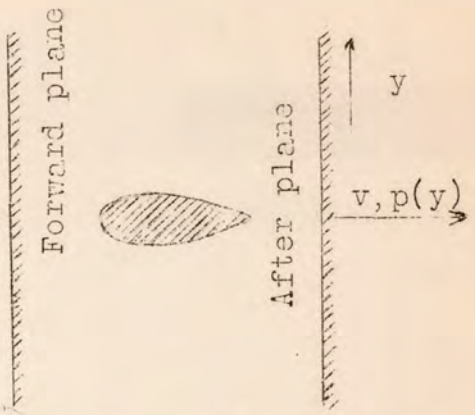

Fig. 2 Application of the law of momentum

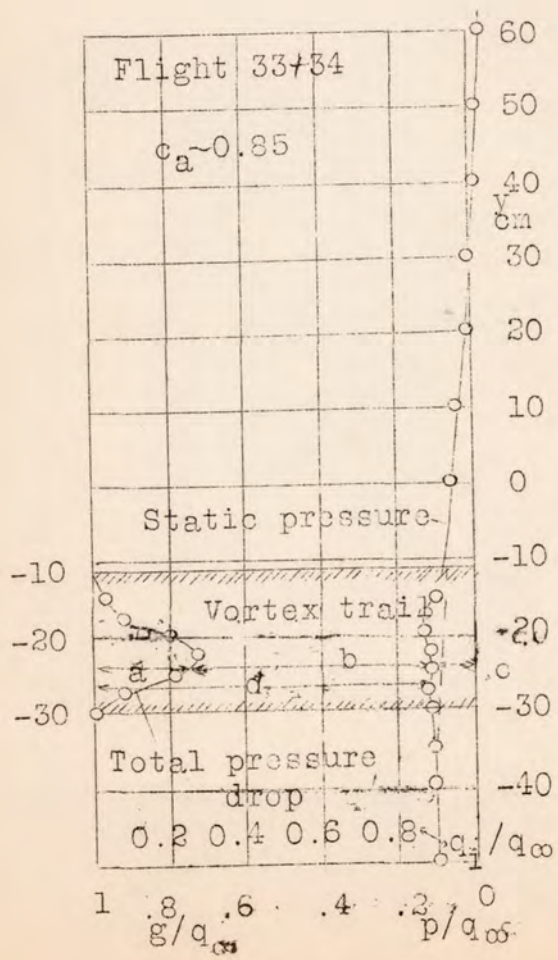

Fig. 3 Pressure conditions behind wing. Left, total pressure, right, static pressure. Elevation (y) of static tube in cm, plotted as ordinate. The points are mean values of 5 to 8 individual measurements.

$a = \frac{g_o - g}{q_\infty}$

$b = q/q_\infty$

$c = p/q_\infty$

$d = q_i/q_\infty$

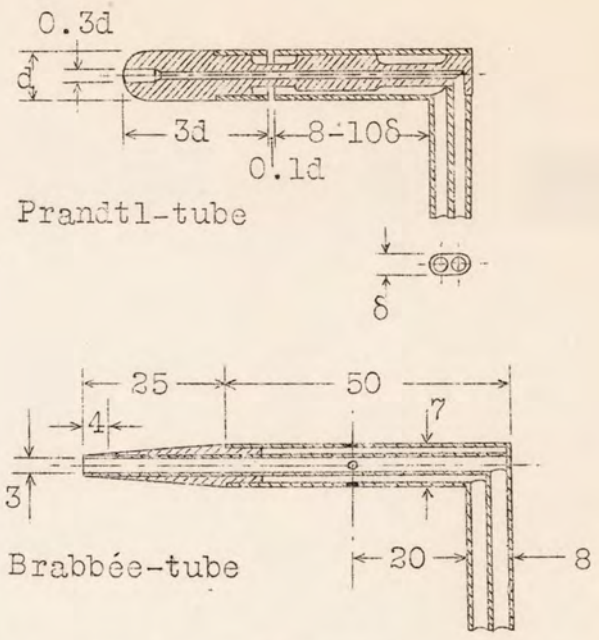

Fig.4 Static tubes used. Prandtl tube. Brabbée tube.

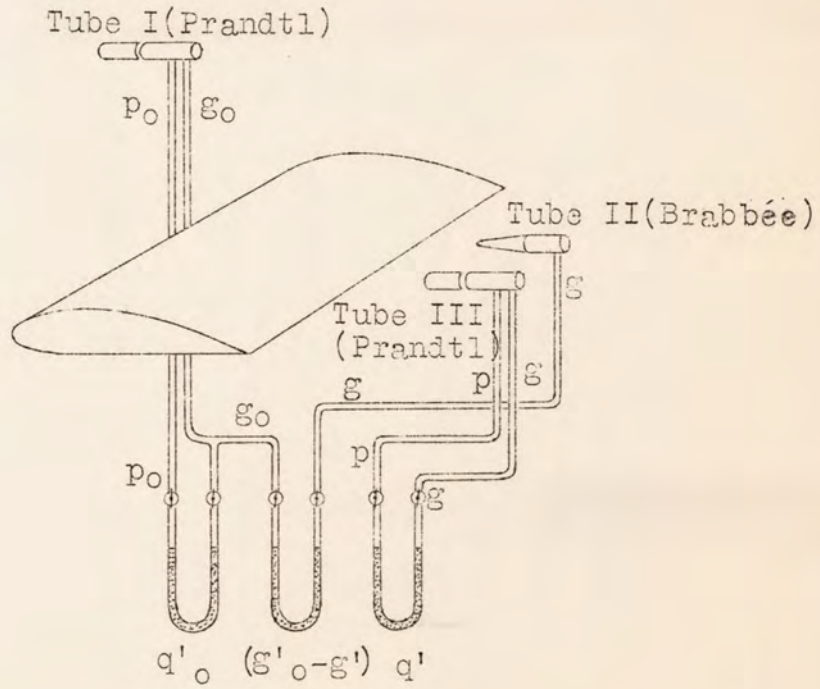

Fig.5 Arrangement of pipes. Forward of and above the wing a Prandtl tube for measurement of undisturbed flow. Behind the wing, in the turbulent region, a Prandtl and a Brabbée tube.

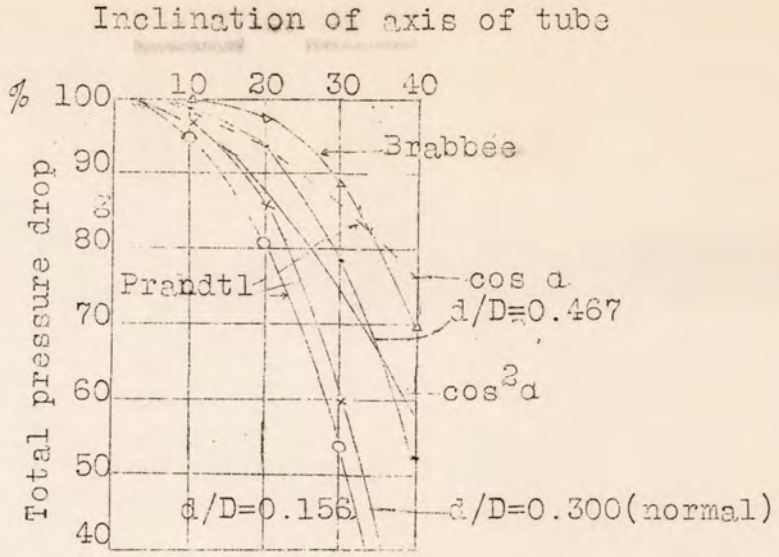

Fig. 6. Angular behavior of different Pitot tubes. The lines are plotted for cosα and $\cos^2\alpha$. Up to a deflection of 20° latter agrees well with normal Prandtl tube.

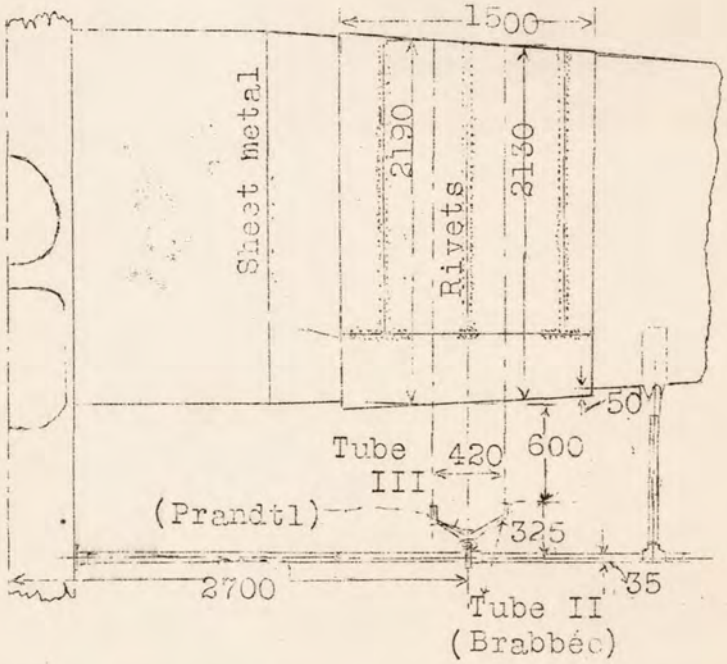

Fig. 7. Installation of covering and Pitot tubes. Position of rivets indicated.

Fig.8 Mounting of front Pitot tube. The Prandtl tube is mounted 4 m above wing on braced mast.

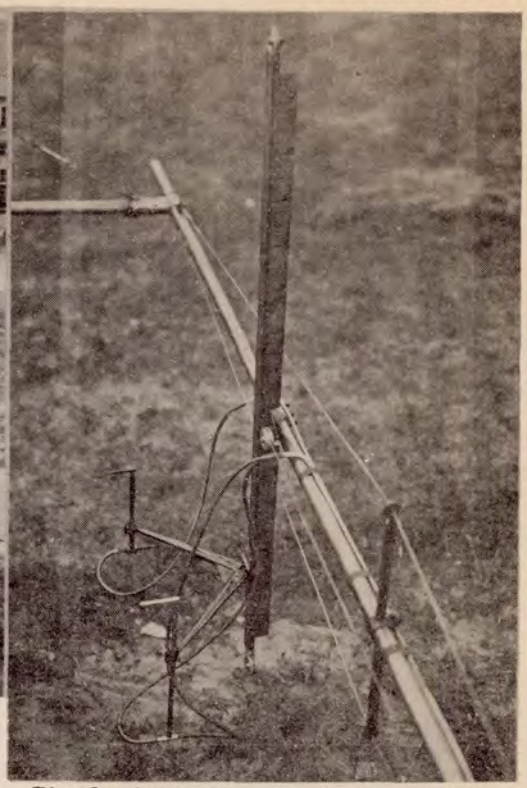

Fig.9 Arrangement of rear Pitot tubes as seen from observer's cockpit. The tubes and their supports are adjustable from the pilot's cockpit.

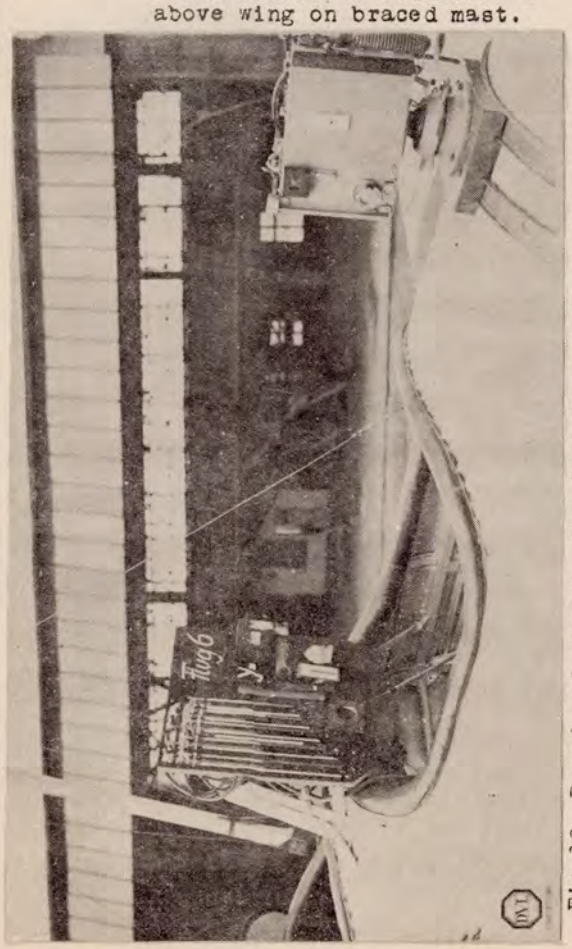

Fig.10 Board and camera. The Askania motion-picture camera is operated from the cockpit by a flexible shaft. Its vibration-proof mounting was particularly difficult.

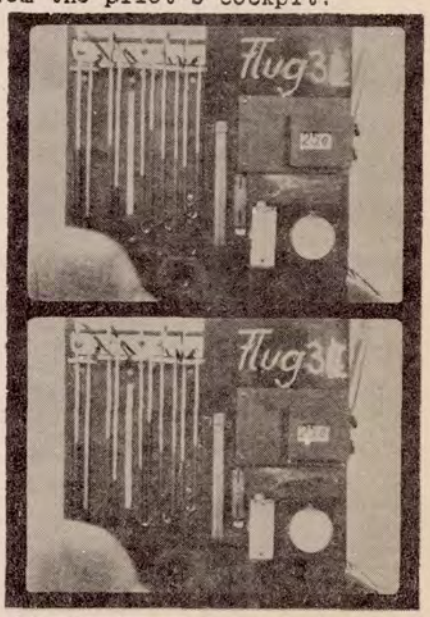

Fig.11 Motion pictures. From left to right the U tubes indicate: undisturbed dynamic pressure, dynamic pressure in turbulent region, disconnected tube, inclinometer, total pressure. The position of the tubes is shown in the roller box.

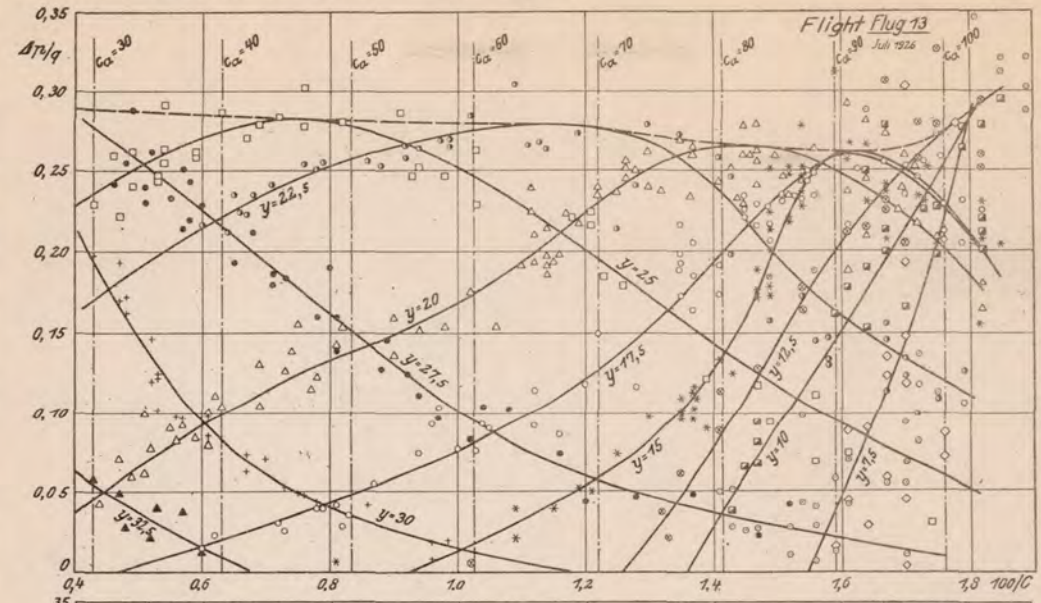

Fig.12 Junkers corrugated sheet metal.

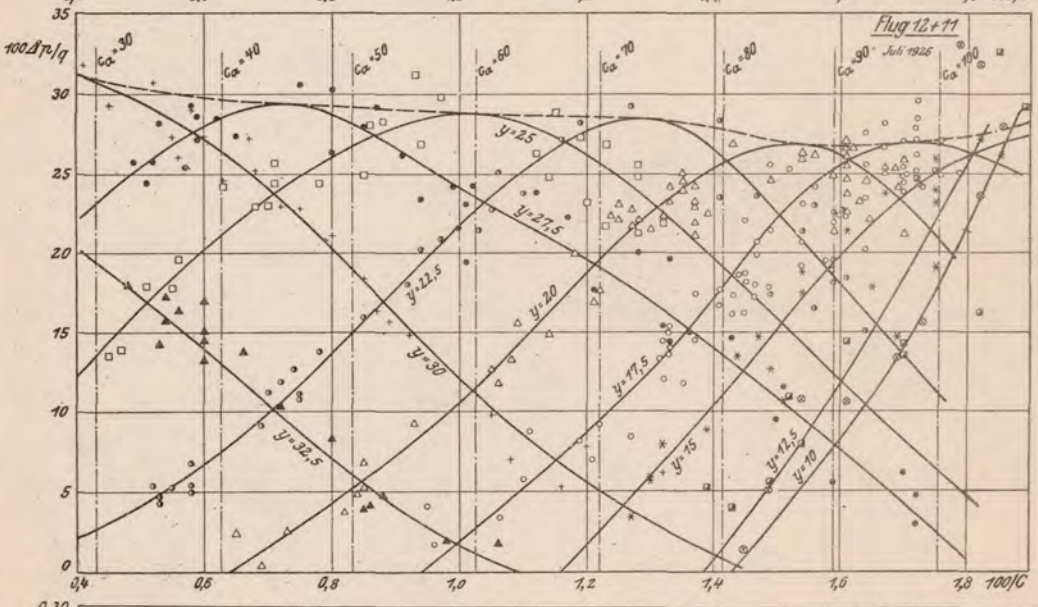

Fig.13 0.5 mm sheet aluminum, wavy and battered.

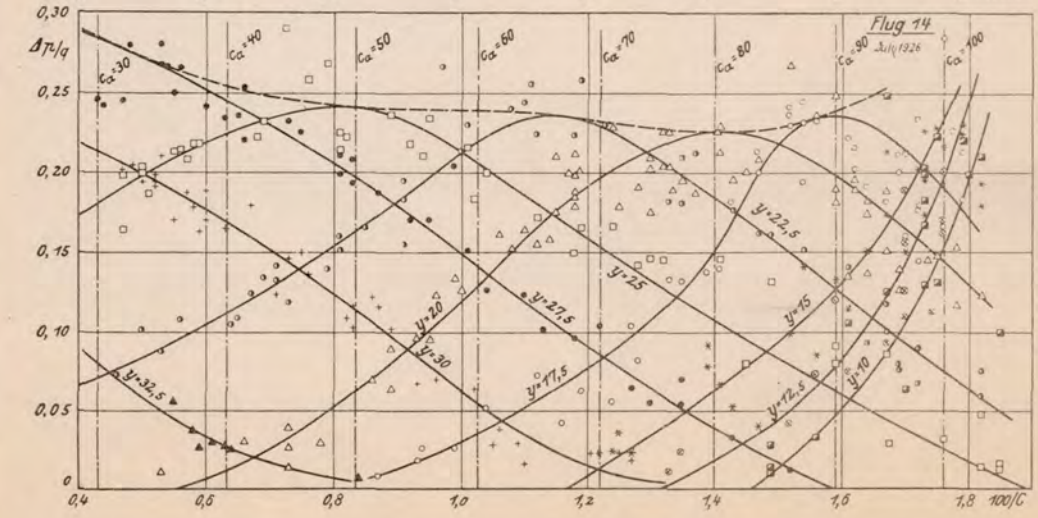

Fig.14 Plywood covering II, oiled.

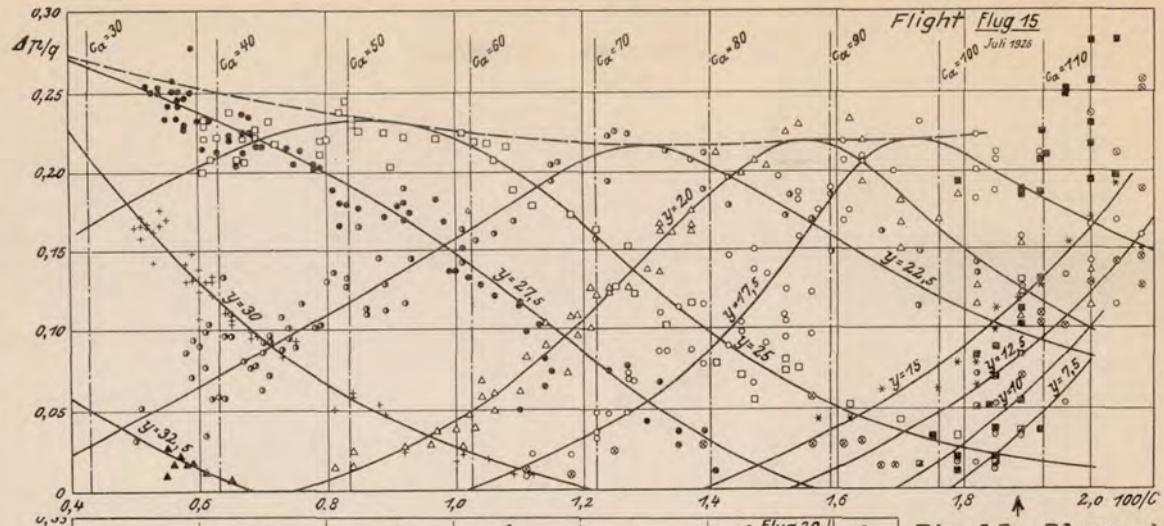

Fig.15 Plywood covering, varnished and polished.

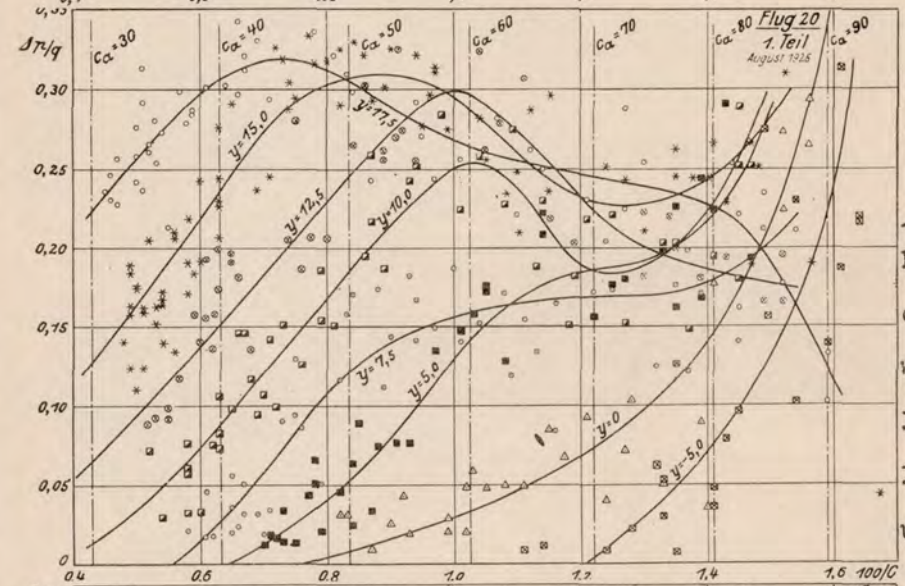

Fig.16 Plywood covering II with fabric, loose and slightly undulating on upper surface.

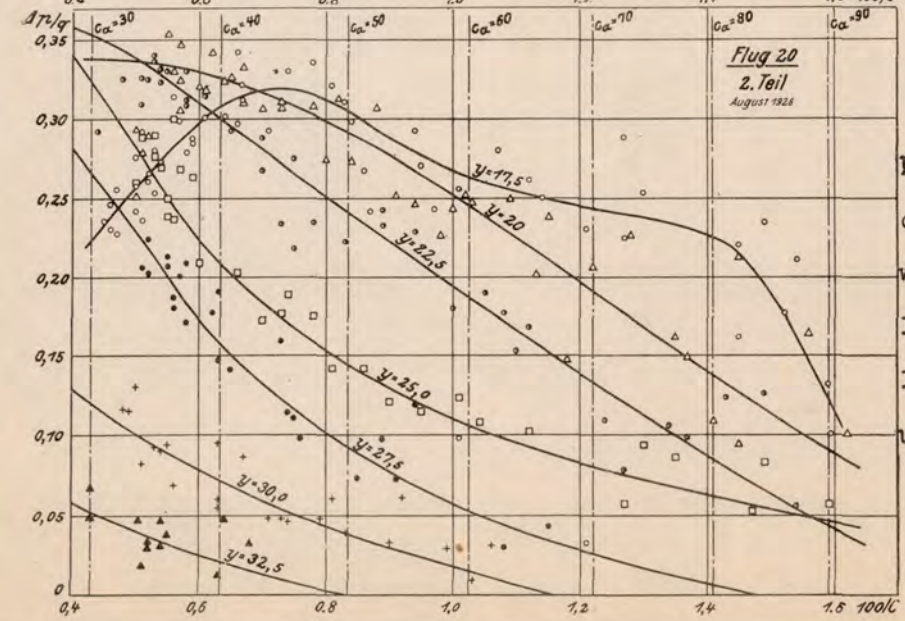

Fig.17 Plywood covering II with fabric, loose and slightly undulating on upper surface.

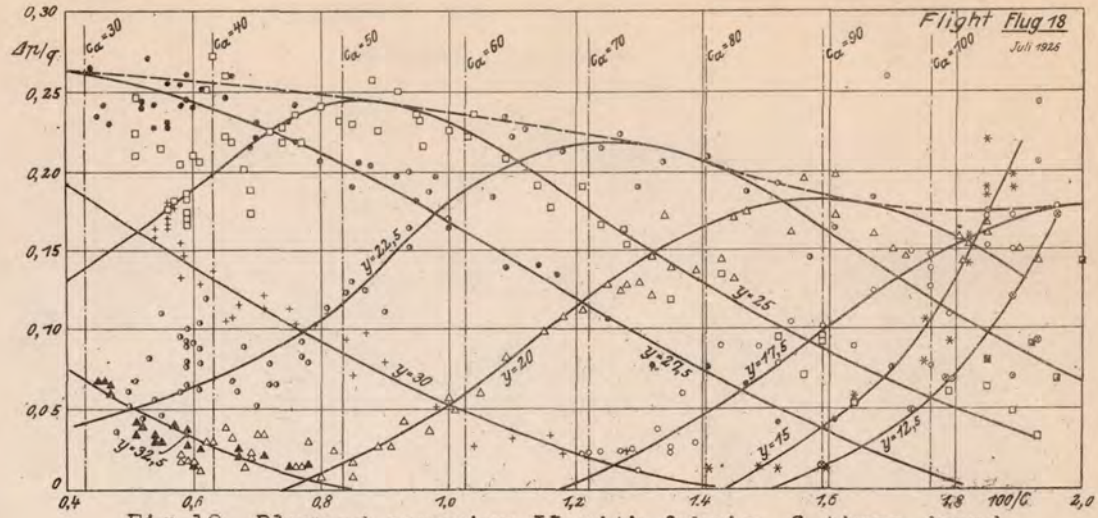

Fig.18 Plywood covering II with fabric, 6 times doped and polished.

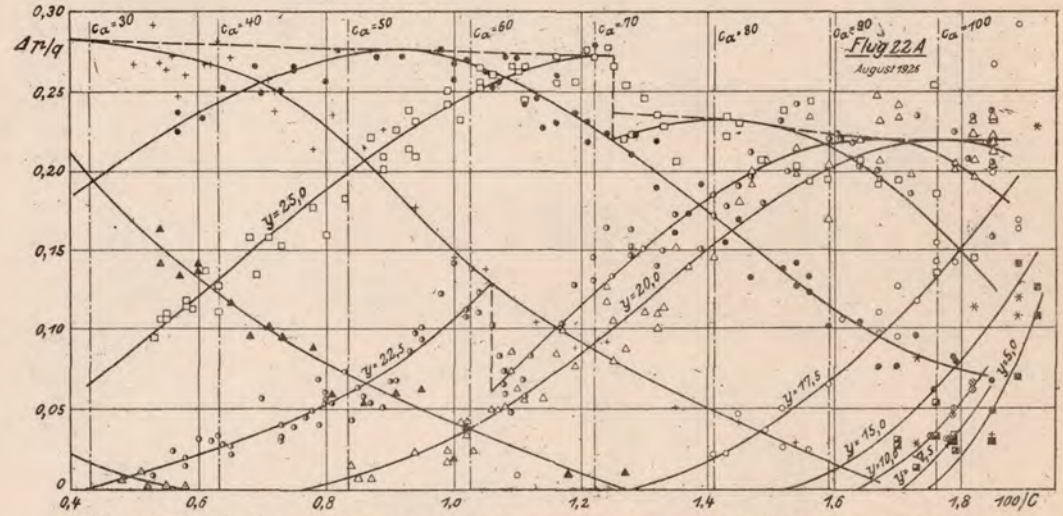

Fig.19 0.9 mm sheet duralumin with rivet heads, smooth.

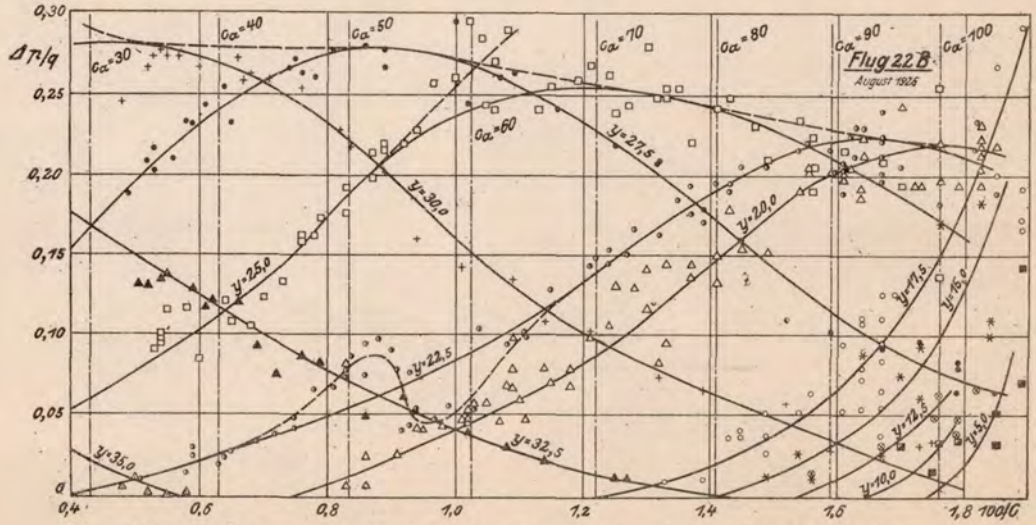

Fig.20 0.9 mm sheet duralumin with rivet heads, smooth.

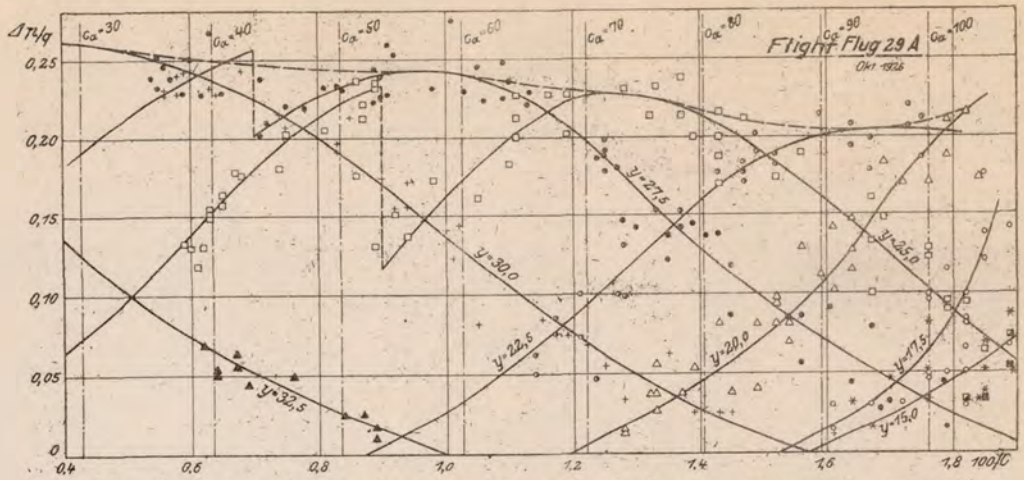

Fig.21 0.9 mm sheet duralumin, rivet heads removed, smooth.

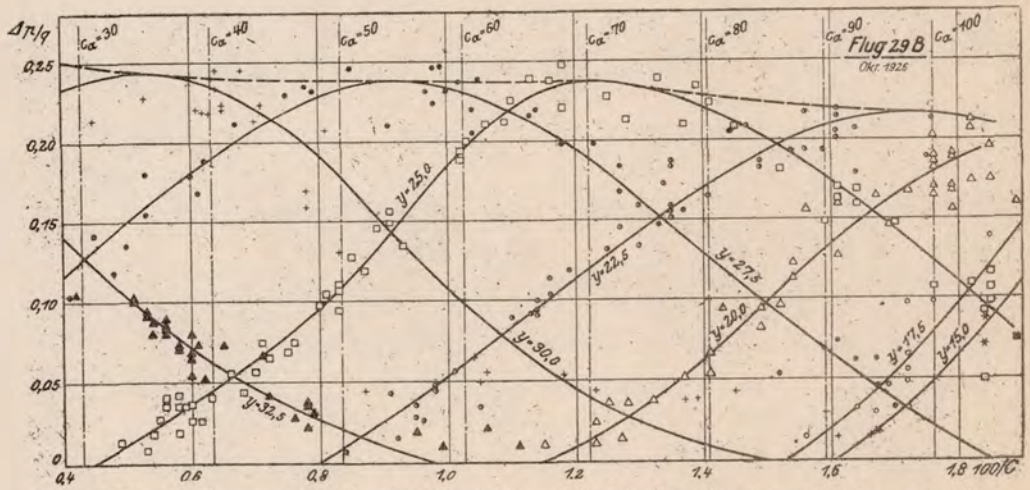

Fig.22 0.9 mm sheet duralumin, rivet heads removed, smooth.

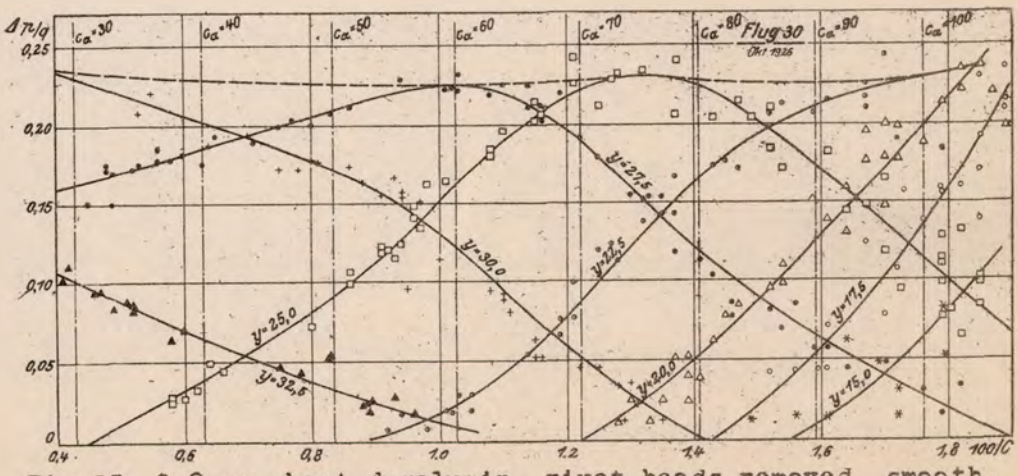

Fig.23 0.9 mm sheet duralumin, rivet heads removed, smooth. Prandtl tube alone, on the right.

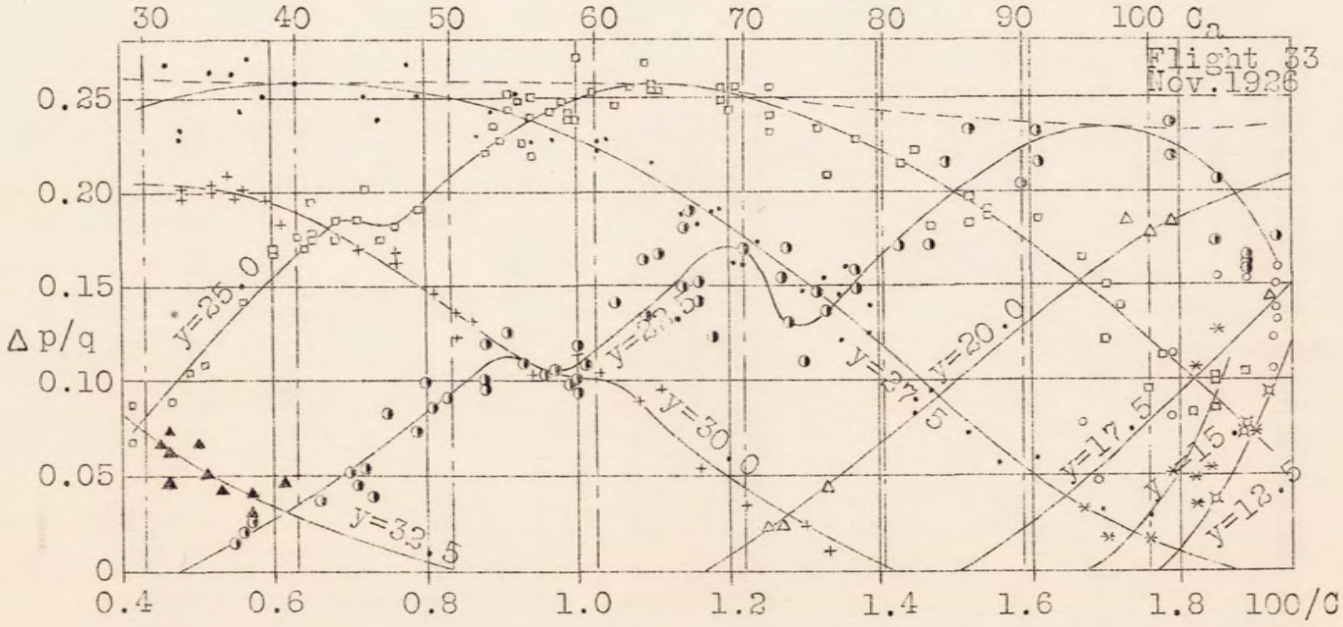

Fig.24 0.9 mm sheet duralumin, rivet heads removed, with aluminum bronze paint. Figs.25 to 36. Second plotting, pressure loops.

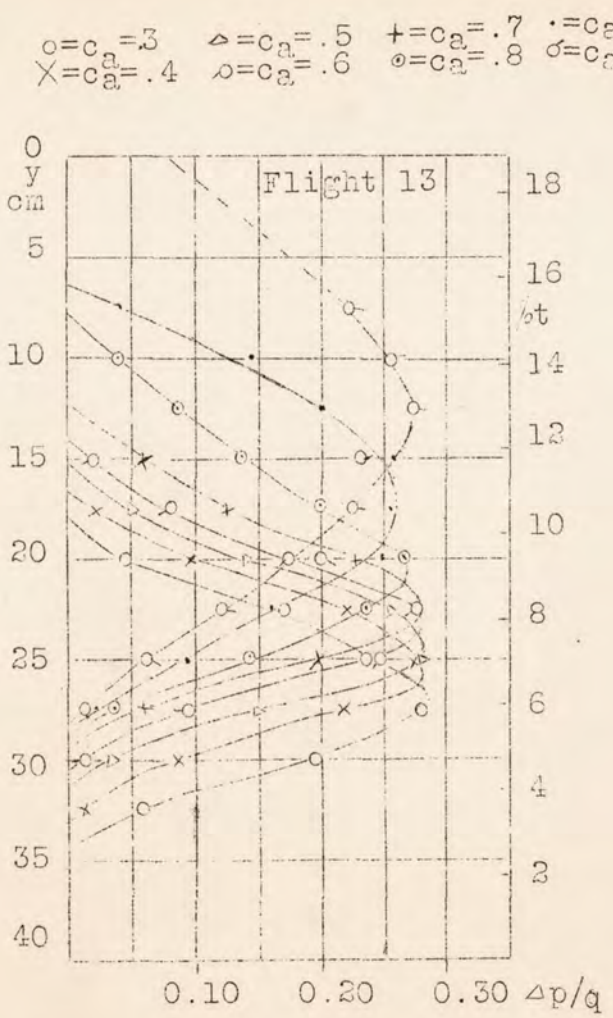

Fig. 25. Junkers corrugated sheet metal.

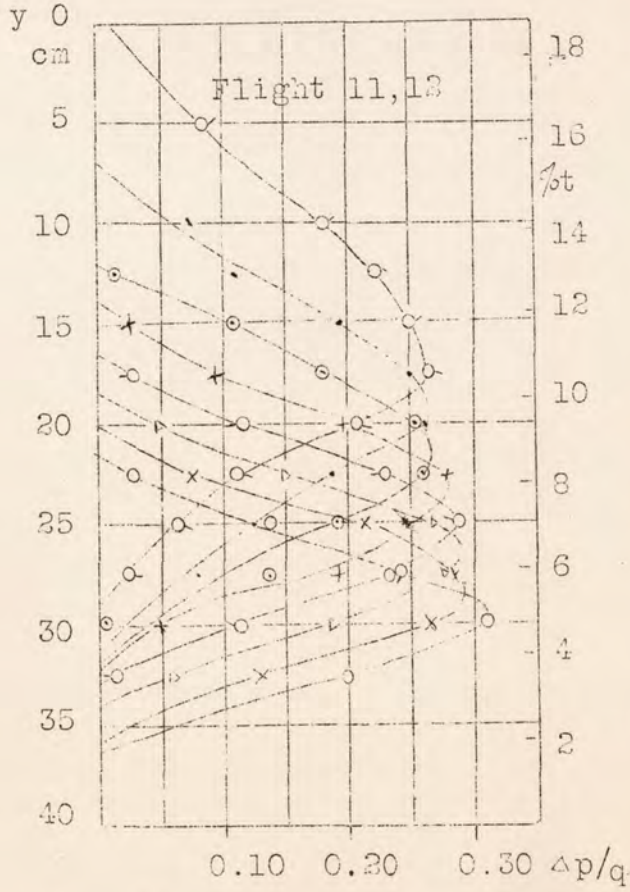

Fig. 26. 0.5 mm sheet aluminum, wavy and battered.

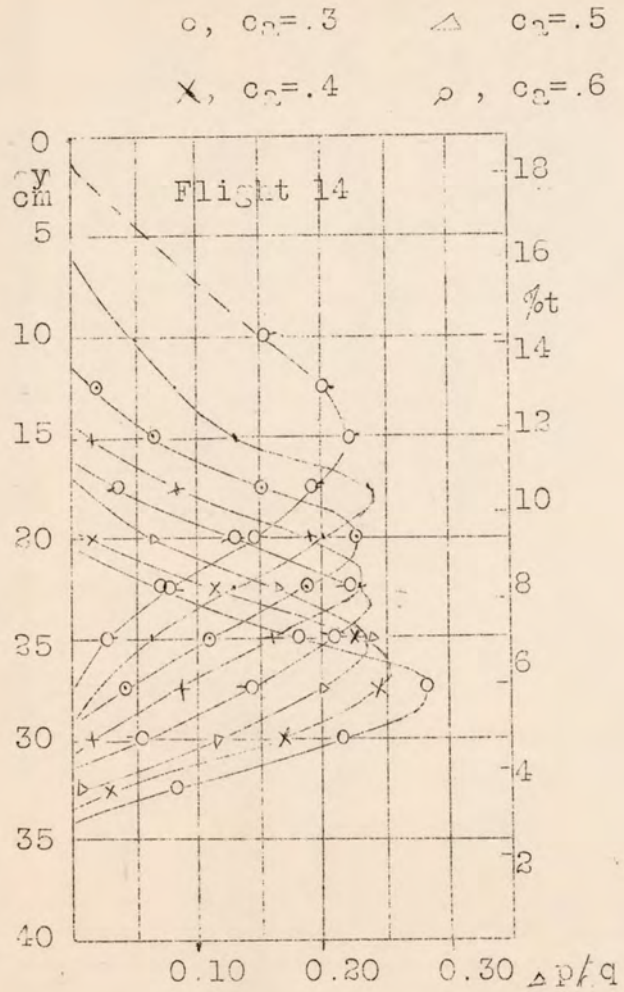

Fig. 27. Plywood covering II, oiled.

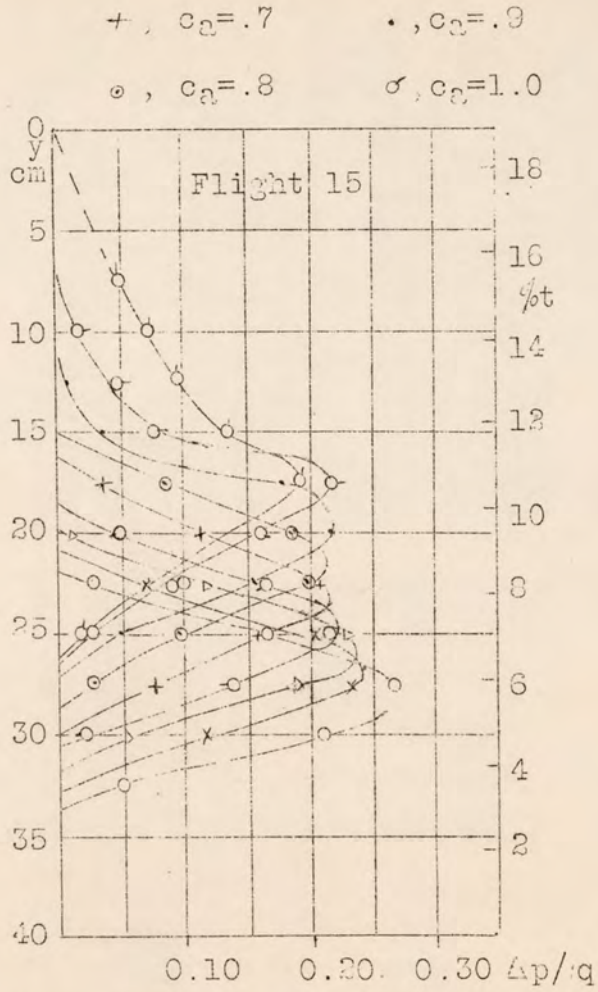

Fig. 28. Plywood covering II, varnished and polished.

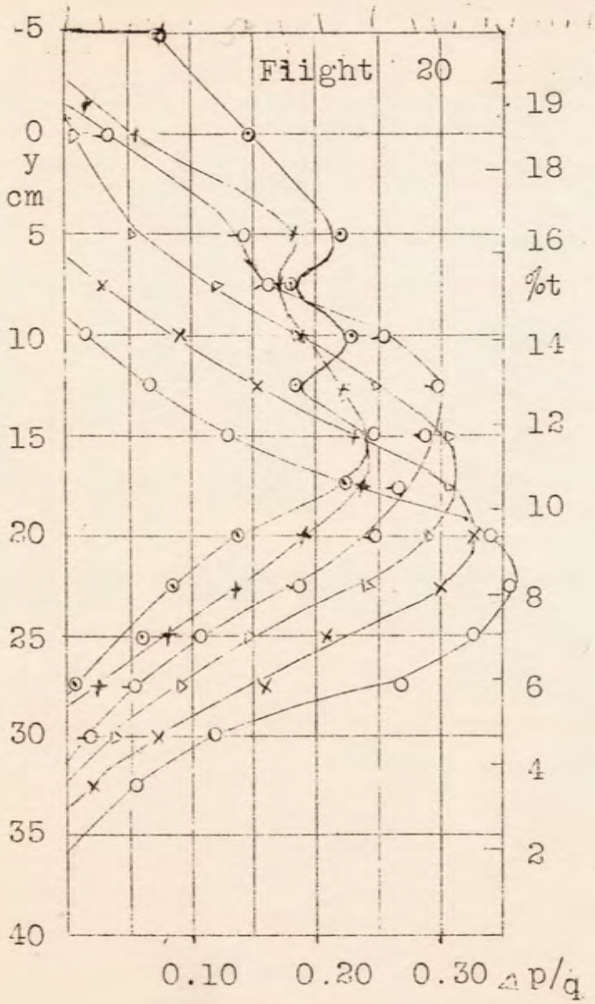

Fig. 29. plywood covering II, with fabric, loose and slightly undulating on upper suface.

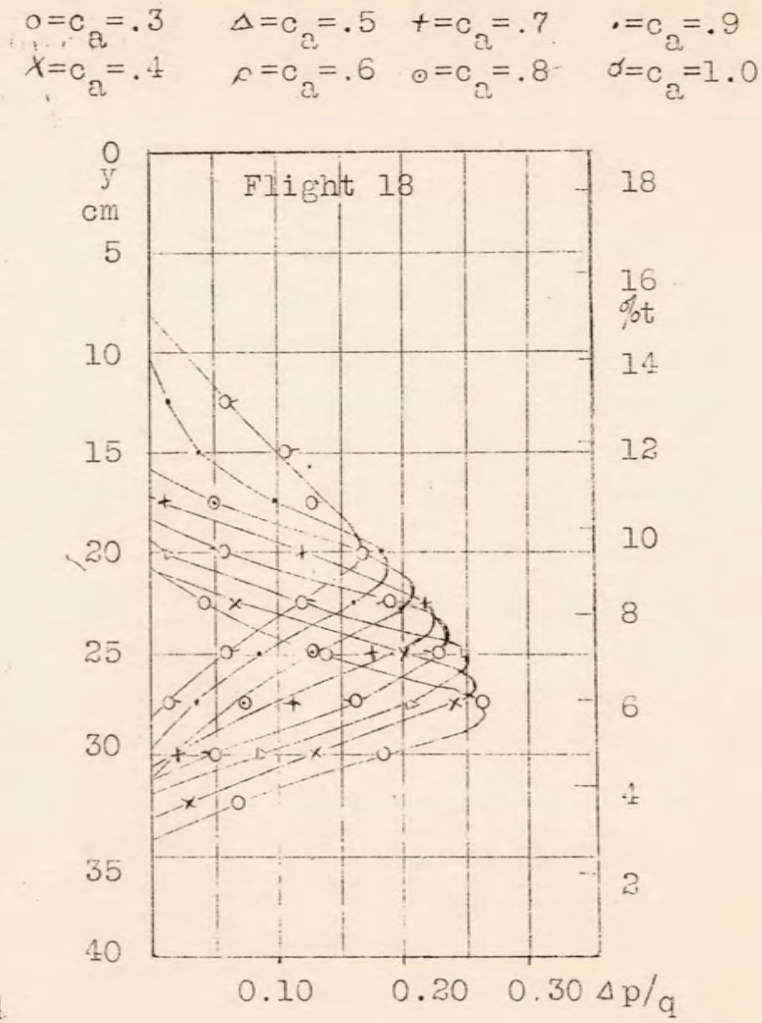

Fig. 30. Plywood covering II with fabric, 6 times doped and smoothed.

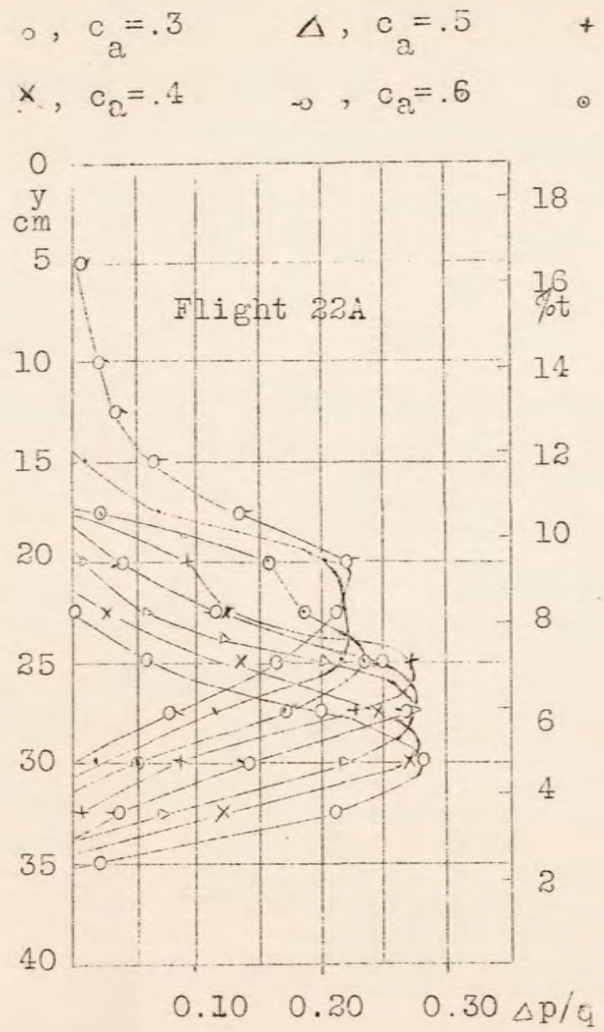

Fig. 31. 0.9 mm sheet duralumin with rivet heads, smooth.

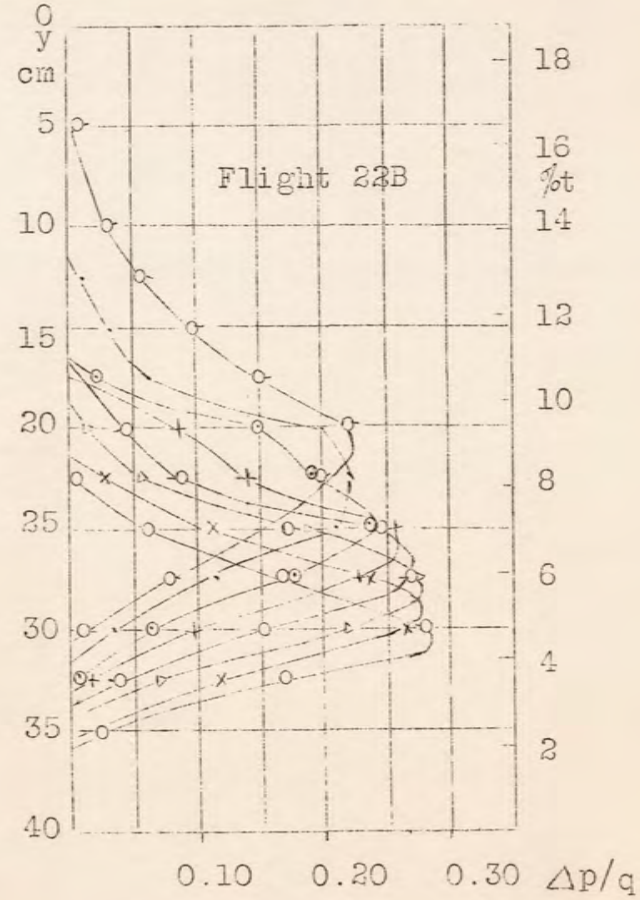

Fig. 32. 0.9 mm sheet duralumin with rivet heads, smooth.

o, c_a = .3 Δ, c_a = .5 +, c_a = .7 •, c_a = .9

x, c_a = .4 ⊖ c_a = .6 ⊙, c_a = .8 ○, c_a = 1.0

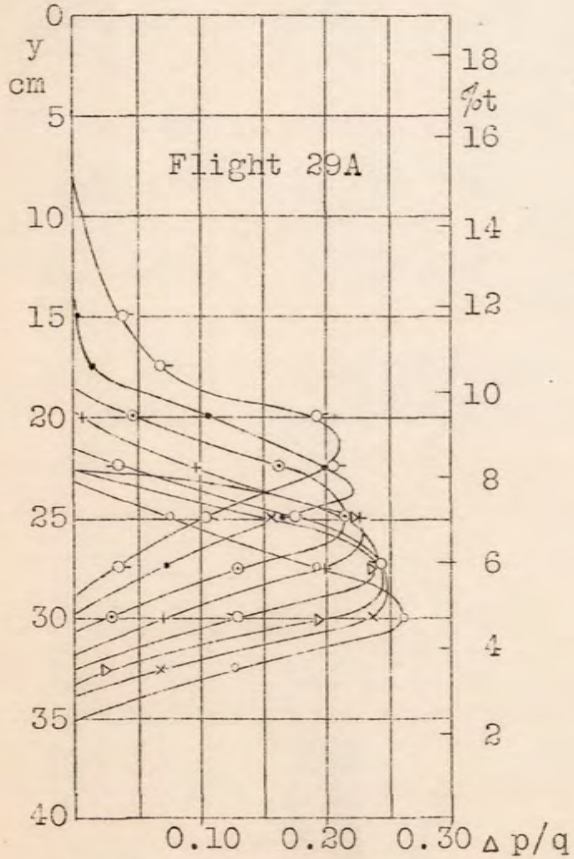

Fig.33 0.9 mm sheet duralumin, rivet heads removed, smooth.

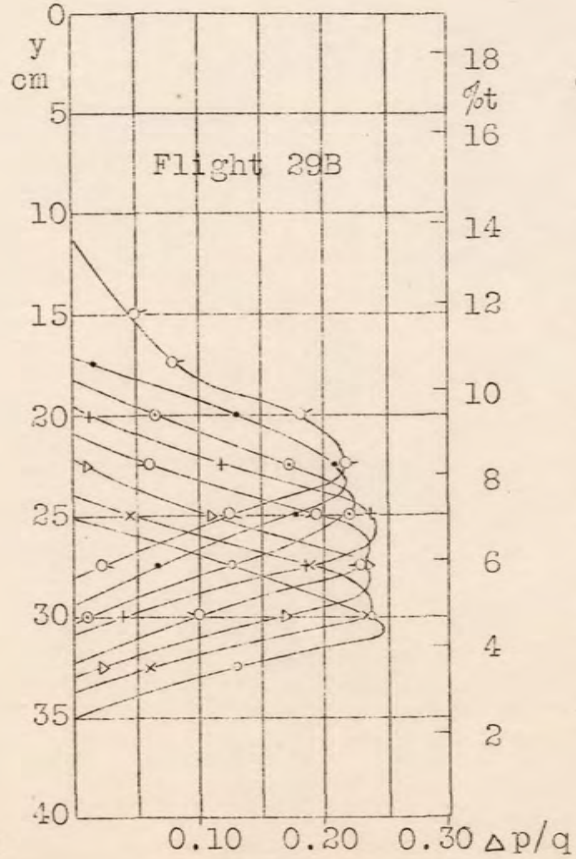

Fig.34 0.9 mm sheet duralumin, rivet heads removed, smooth.

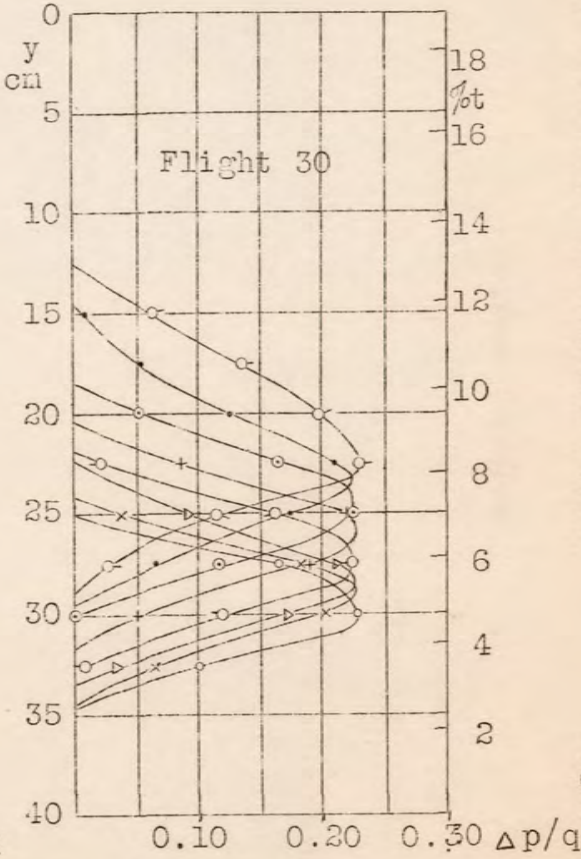

Fig.35 0.9 mm sheet duralumin, rivet heads removed, smooth.

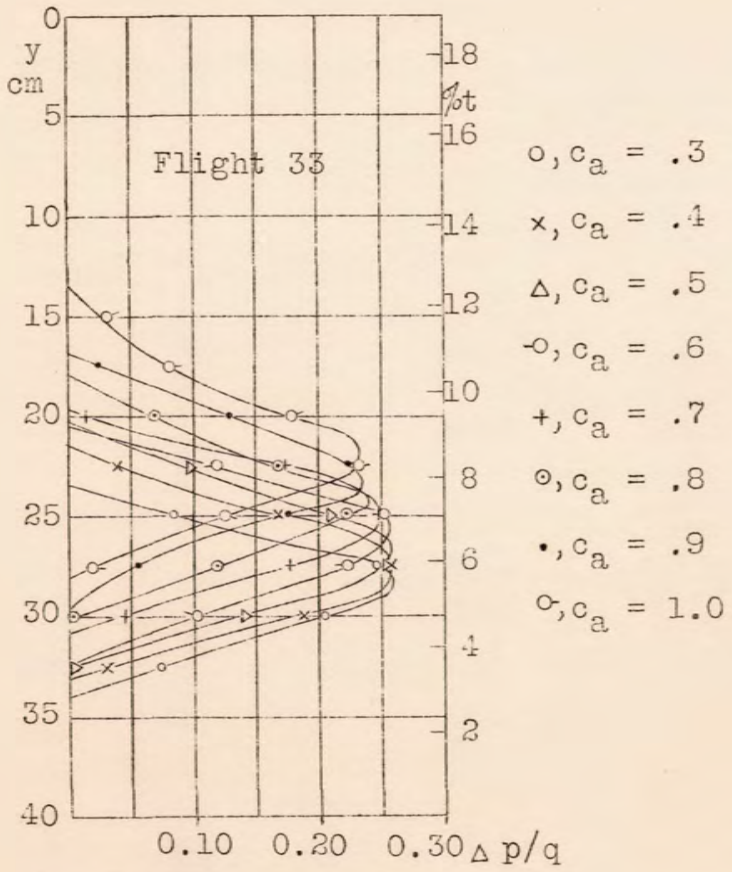

Fig.36 0.9 mm sheet duralumin, rivet heads removed, with aluminum-bronze paint.

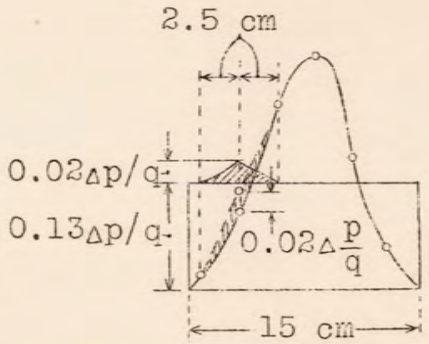

Fig.37 Error estimation.

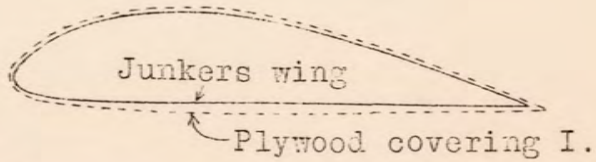

Junkers wing d/t = 0.173
Plywood wing d/t = 0.191

Fig.38 Tested wing sections.

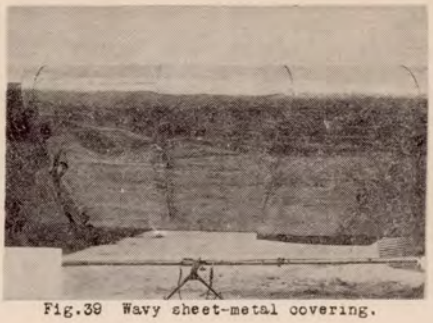

Fig.39 Wavy sheet-metal covering.

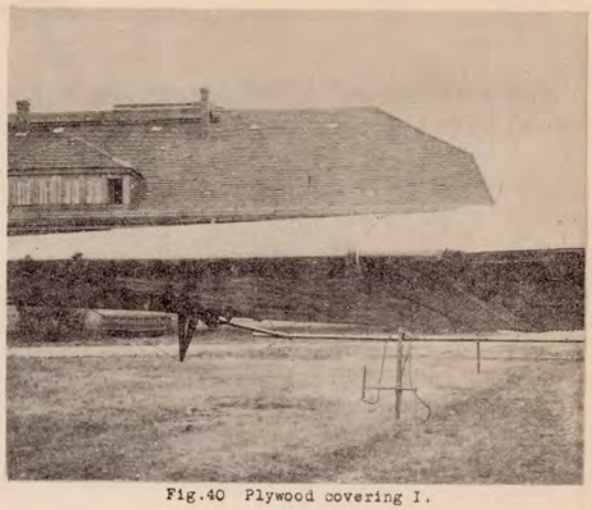

Fig.40 Plywood covering I.

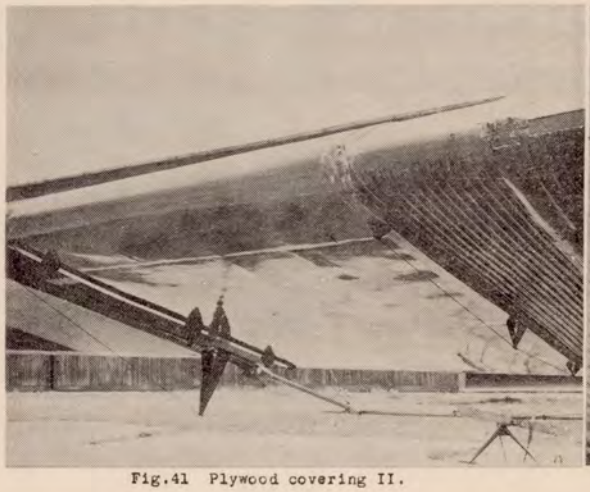

Fig.41 Plywood covering II.

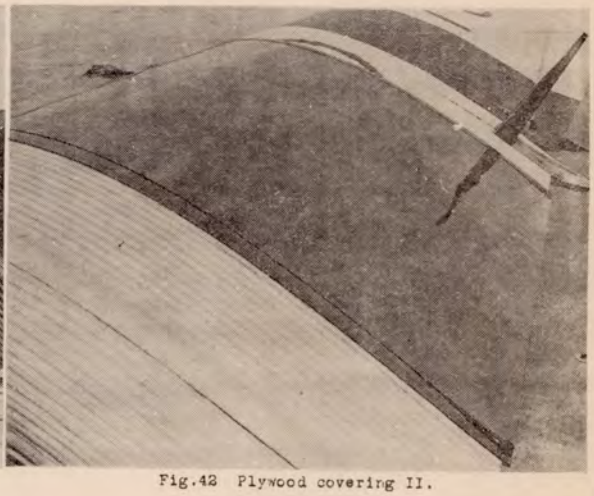

Fig.42 Plywood covering II.

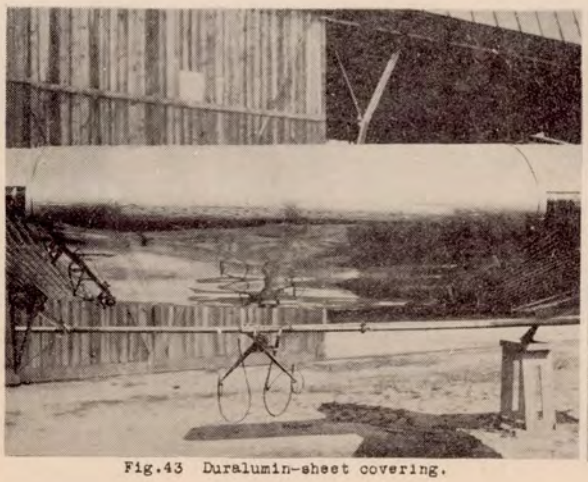

Fig.43 Duralumin-sheet covering.

Fig.44 Duralumin-sheet covering.

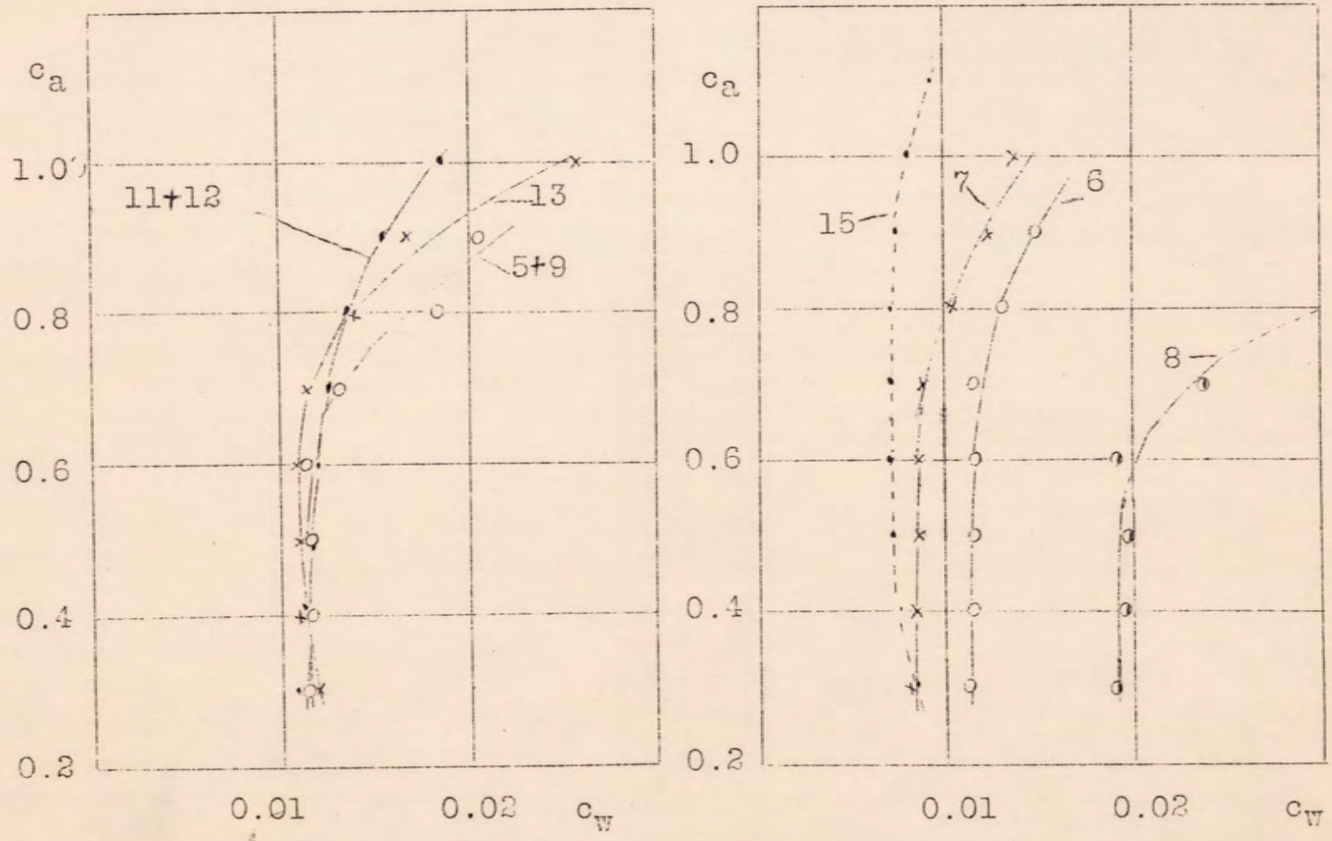

Fig. 45. Polars. Flight 5+9 Junkers corrugated sheet metal. Flight 11+12, 0.5 mm sheet aluminum wavy. Flight 13 Junkers corrugated sheet metal.

Fig.46 Polars. Flight 6, plywood covering I, oiled. Flight 7, plywood covering I, varnished. Flight 8, plywood covering I, roughened with poppy seed. Flight 15, plywood covering II, varnished and polished.

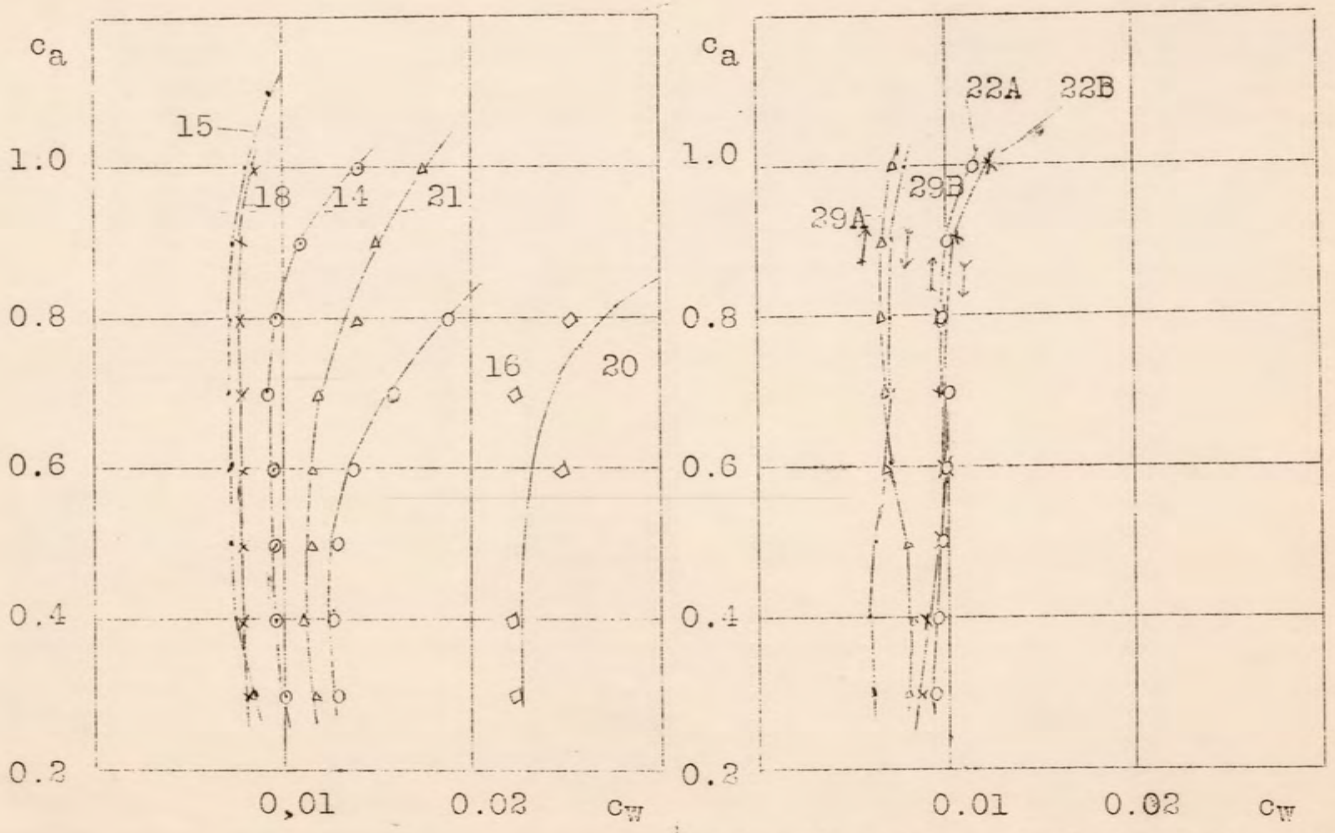

Fig. 47 Polars with plywood covering.

Flight 14, II, oiled.
Flight 15, II, varnished and polished.
Flight 16, II, with coarse fabric taut.
Flight 18, II, with fabric 6 times doped and polished.
Flight 20, II, with fabric on upper surface loose.
Flight 21, II, with fabrics twice doped, slightly polished.

Fig. 48. Polars. Flight 22 A and B, 0.9 mm sheet duralumin with rivet heads, smooth. Flight 39 A and B, 0.9 mm sheet duralumin with rivet heads removed, smooth.

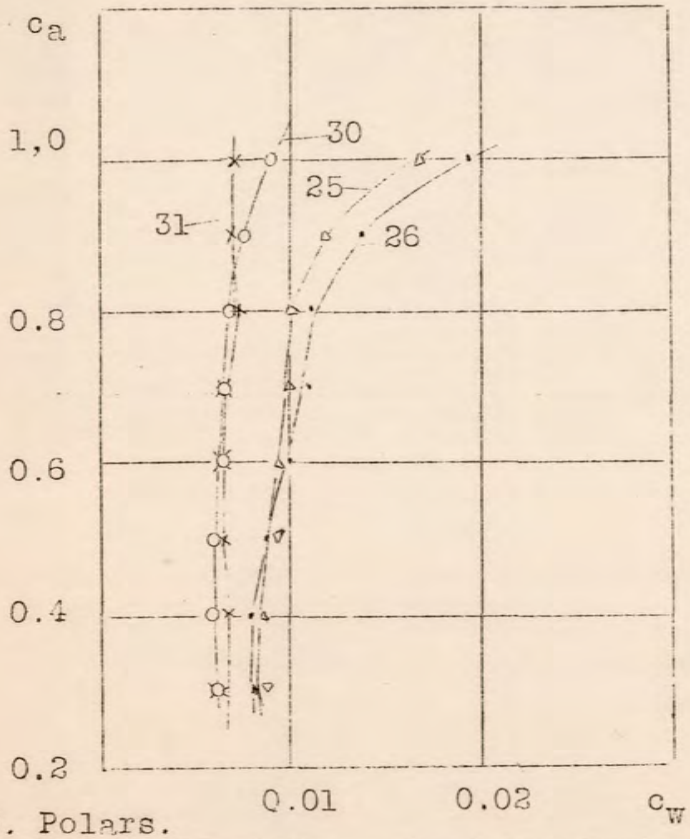

Fig.49. Polars.

Flight 25, 0.9 mm sheet duralumin with rivet heads and aluminum-bronze paint, Prandtl tube alone on the right. Flight 26, 0.9 mm sheet duralumin with rivet heads and aluminum-bronze paint, Prandtl tube alone on the left. Flight 30, 0.9 mm sheet duralumin rivet heads removed, smooth, Prandtl tube alone on the right. Flight 31, 0.9 mm sheet duralumin, rivet heads removed, smooth, Prandtl tube alone on the left.

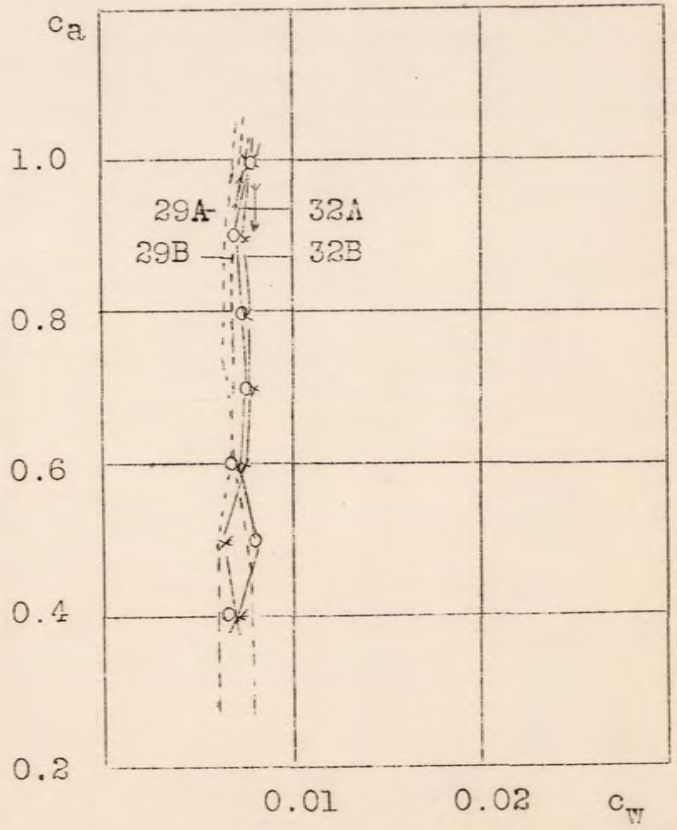

Fig.50. Polars. Flight 29A and 29B, 0 9 mm sheet duralumin, rivet heads removed, smooth. Flight 33A and 33B, 0.9 mm sheet duralumin, rivet heads removed, smooth.

Figs. 49, 50.

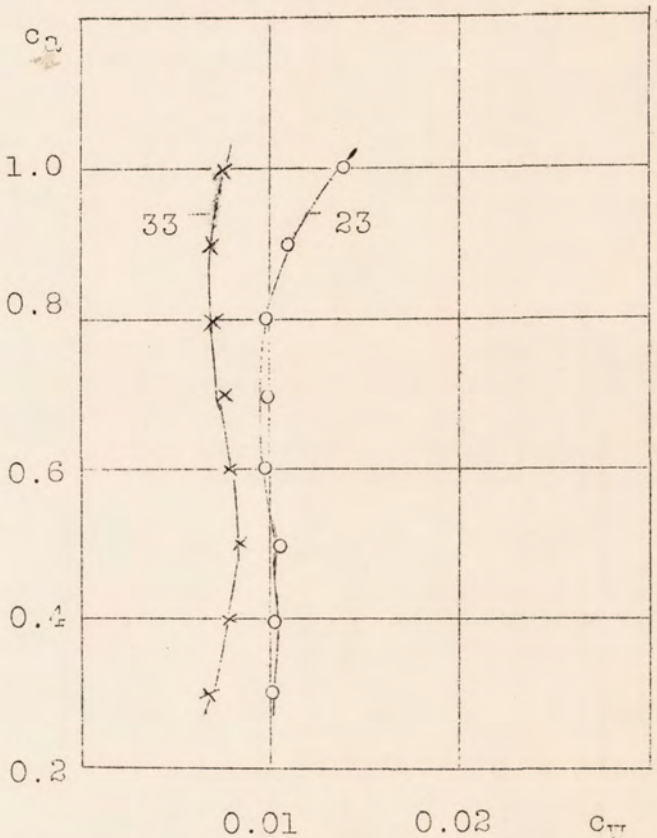

Fig.51. Polars. Flight 23, 0.9 mm sheet duralumin with rivet heads and aluminum-bronze paint. Flight 33, 0.9 mm sheet duralumin, rivet heads removed, with aluminum-bronze paint.